Alpha, Beta and Gamma Dose Rates in Water in Contact with Used CANDU Fuel

NWMO TR-2009-27 **November 2009**

F. Garisto[1], D.H. Barber[2], E. Chen[2], A. Inglot[2] and C.A. Morrison[2]

[1]Nuclear Waste Management Organization

[2]AMEC NSS

nwmo
NUCLEAR WASTE MANAGEMENT ORGANIZATION
SOCIÉTÉ DE GESTION DES DÉCHETS NUCLÉAIRES

Nuclear Waste Management Organization
22 St. Clair Avenue East, 6th Floor
Toronto, Ontario
M4T 2S3
Canada

Tel: 416-934-9814
Web: www.nwmo.ca

Alpha, Beta and Gamma Dose Rates in Water in Contact with Used CANDU Fuel

NWMO TR-2009-27

November 2009

F. Garisto[1], D.H. Barber[2], E. Chen[2], A. Inglot[2] and C.A. Morrison[2]

[1]Nuclear Waste Management Organization

[2]AMEC NSS

ABSTRACT

Title: **Alpha, Beta and Gamma Dose Rates in Water in Contact with Used CANDU Fuel**
Report No.: **NWMO TR-2009-27**
Author(s): F. Garisto[1], D.H. Barber[2], E. Chen[2], A. Inglot[2] and C.A. Morrison[2]
Company: [1]Nuclear Waste Management Organization, [2]AMEC NSS
Date: November 2009

Abstract
The Canadian concept for a geological repository for used fuel is based on multiple barriers, including the used UO_2 fuel itself. In the event of failure of the fuel container, groundwater would enter the container and contact the fuel, after the Zircaloy cladding is breached. Since more than 95% of the radionuclide inventory in used fuel is trapped within the fuel grains, the long-term release of radionuclides from the fuel is controlled by the dissolution of the used fuel.

Uranium dioxide has a low solubility under the reducing conditions expected in a deep geological repository and thus dissolves very slowly under such conditions. However, the radiolysis of groundwater, caused by the radiation emitted by used fuel, generates oxidants (e.g., H_2O_2) that can react with the fuel and dissolve it. Thus, the rate of dissolution of the fuel in a failed container is expected to be controlled by the rate of generation of oxidants by radiolysis of groundwater, until the radiation fields have decayed to sufficiently low levels. Consequently, it is important to have good estimates of the alpha, beta and gamma dose rates near the fuel surface.

The purpose of this report is to document the calculation of the alpha, beta and gamma dose rates in water in contact with a used fuel bundle, given the radionuclide inventories in used fuel. These dose rates are provided as a function of time for decay times from 10 to 10^7 years after discharge.

Based on the work described in this report the following additional conclusions can be made:

1. The appropriate value of the relative stopping power of alpha particles for water relative to uranium dioxide is 3.25.
2. The beta energy emitted by fuel is generated mainly by fission products for decay times up to about 200 years. The contribution from beta decay of the actinides and their progeny becomes significant after 200 years and is dominant for decay times greater than 300 years. However, by this time, the beta dose rate is much smaller than the alpha dose rate.
3. For gamma radiation, the F-factor is defined as the ratio of the gamma dose rate in water near a fuel bundle in a used fuel container to the corresponding dose rate from a single bundle in an infinite pool of water. The weighted average F-factors for the reference container ranged from 1.22 to 1.38, depending on the decay time. A value of 1.4 is recommended for safety assessment calculations.

TABLE OF CONTENTS

LIST OF TABLES

Page

LIST OF FIGURES

Page

1. INTRODUCTION

In the Canadian approach to the long-term management of used nuclear fuel, used fuel will be isolated in a deep geological repository located in a suitable rock formation (NWMO 2005). The repository concept is based on multiple barriers, including the UO_2 fuel itself, the fuel container, the buffer backfill and the geosphere.

In the event of failure of the fuel container, groundwater would enter the container and contact the fuel after the Zircaloy cladding is breached. Since most (>95%) of the radionuclides in used fuel are bound within the UO_2 fuel grains, the long-term release of radionuclides from used fuel is controlled by the dissolution rate of the fuel matrix.

Uranium dioxide has a low solubility under the reducing conditions expected in a deep geological repository and thus dissolves very slowly under such conditions. However, the radiolysis of groundwater, caused by the radiation emitted by used fuel, generates oxidants (e.g., H_2O_2) that can react with the fuel and dissolve it. Thus, the rate of dissolution of the fuel in a failed container is expected to be controlled by the rate of generation of oxidants by radiolysis of groundwater, until the radiation fields have decayed to sufficiently low levels. Consequently, it is important to have good estimates of the alpha, beta and gamma dose rates in water near the fuel surface.

In the safety assessment models used in recent Canadian case studies, notably the Third Case Study (TCS) (Garisto et al. 2004, Appendix E), the rate of dissolution of the used UO_2 fuel is directly related to the alpha, beta and gamma dose rates near the fuel surface.

The purpose of this report is to document the calculation of the dose rates in water arising from the alpha, beta and gamma decay of used CANDU fuel, based on the radionuclide inventories calculated by Tait et al. (2000).

Section 2 provides some background information, including the definition of terms used in this report. The calculations of the alpha, beta and gamma dose rates are described in Sections 3, 4 and 5, respectively. Section 6 provides the conclusions of this work.

2. BACKGROUND

The radionuclide inventories provided by Tait et al. (2000) were used in the calculations of the alpha, beta and gamma dose rates in water adjacent to the surface of used CANDU fuel. These inventories were calculated, based on the fuel composition and known or assumed initial levels of impurities in fuel, using the ORIGEN-S isotope generation/depletion code.

In conjunction with information on the specific radiation emitted by each radionuclide, principally that given in the radioactive decay data of Kocher (1981), the inventory tabulations were used to determine the fraction of decay energy that is emitted as alpha, beta and gamma energy.

The gamma photon spectra of the used fuel, as a function of decay time, provided by Tait et al. were also relevant.

2.1 DEFINITIONS

For each fuel burnup value (220, 280 and 320 MWh/kgU), the radionuclide inventory tables in Tait et al. (2000) are divided into 3 main parts: those for actinides, fission products and light element impurities. These terms, which are used in the discussions in this report, are defined in this section.

Actinides: In this report the term actinide refers to heavy elements of atomic number greater than 89 and their decay products.

Actinide Decay Chains: The actinides can be divided into four decay chains. The chains are characterized by the values 4n, 4n+1, 4n+2 and 4n+3. The chains were named after prominent elements in the chain. They are the thorium series (Th-232), the neptunium series (Np-237), the uranium series (U-238) and the actinium series (Ac-227), respectively. The actinide decay chains end when reaching a stable nuclide of lead or bismuth. Outside a reactor, it is very unlikely for an actinide to cross over into another decay chain.

Fission Products: In nuclear fission, the nucleus of a fissile nuclide splits into two (or occasionally three) new nuclei. The new nuclides formed in this way are referred to as fission products. The ternary fission products have very low atomic number ranging from 1 (hydrogen) to about 6 (carbon). The remaining fission products have atomic numbers between about 29 (copper) and about 68 (erbium). The distribution of fission product yields is bimodal with peaks at mass numbers of approximately 95 and 135.

Light Elements: Referred to as light element impurities by Tait et al. (2000), this group of radionuclides consists of those elements that are initially present as impurities in the nuclear fuel or are produced, while the fuel was in the reactor, from these impurities by nuclear activation.

Decay Time: The term decay time is used in this report to denote the fuel age or elapsed time since discharge of the used fuel from an operating reactor.

2.2 GENERAL ACTINIDE AND FISSION PRODUCT PROPERTIES

For the decay of an actinide of atomic number Z_a and mass number M_a to a stable lead or bismuth nuclide of atomic number Z_s and mass number M_s, the number of alpha decays can be determined to be $(M_a - M_s)/4$. The number of beta decays is $(M_a - M_s)/2 - (Z_a - Z_s)$. For example, for the decay of U-238 to Pb-206, there are 8 alpha decays (= (238 – 206)/4) and 6 beta decays ((238 – 206)/2 - (92 – 82)). The presence of long-lived actinides in a decay chain provides an ongoing source for the production of short-lived nuclides. For example, U-238 (half-life of 4.47×10^9 years) is a parent of Po-214 (half-life of 164.3 μs). Thus, even though Po-214 has a very short half-life, its continuing production via decay of U-238 results in an ongoing inventory of Po-214 in secular equilibrium with the long-lived parent.

Fission products tend to lie below the line of beta stability on the chart of the nuclides, and to decay primarily by beta decay. However, a few fission product nuclides (i.e., Ce-142, Nd-144, Sm-146 to Sm-149, and Gd-152) are long-lived alpha emitters. Given the small yield of fission product alpha emitters relative to beta/gamma emitters, their contribution to decay power is a

small fraction of both the total decay power from fission products, and the total alpha decay power for decay times up to 10 million years.

2.3 PREVIOUS WORK

In the Third Case Study (Garisto et al. 2004), simplifying approximations were used to calculate the radiation doses from alpha, beta and gamma radiation in water adjacent to used fuel. These approximations are briefly described below.

For calculation of the alpha decay energy, it was assumed that the alpha decay energy could be approximated by the difference between the total decay energy and gamma decay energy from actinides and their decay products. Following Sunder (1995, 1998), a relative mass stopping power of 1.39 for alpha particles in water versus alpha particles in uranium dioxide was used (see Section 3.2), based on an approximation to the Bethe-Bloch equation (Nitzki and Matzke 1973).

For beta radiation, the assumption was made that the beta decay energy for used fuel could be approximated by the difference between the total decay energy and gamma decay energy of the fission products and light elements. Following Sunder (1995, 1998), a relative mass stopping power of 1.8 was used for beta particles in water versus uranium dioxide.

For gamma radiation, the gamma decay energy for used fuel was approximated as the sum of the gamma decay energies for the actinides, fission products and light elements in the fuel, and the gamma decay energy of the activation products in the Zircaloy cladding. The gamma energy from the Zircaloy is a small fraction of the gamma energy from the fuel.

The conversion of the total gamma decay energy into a gamma dose rate adjacent to the fuel surface was based on data from previous studies (Garisto et al. 2004, Appendix E) that indicated that the ratio of the gamma dose rate at the fuel surface (of a single fuel bundle) to the total gamma decay energy of the fuel bundle is 2.91×10^6 (Gy/a)/(W/kgU).

However, gamma radiation is long ranged. Therefore, in a used fuel container, the gamma radiation from many fuel bundles contributes to the gamma dose rate in water near any particular fuel bundle. The contribution of the other fuel bundles to the gamma dose rate near a fuel bundle is represented by the F-factor, F; that is,

$$D_{g,cont} = F \times D_{g,1} \qquad (2.1)$$

where $D_{g,cont}$ is the average gamma dose rate near a fuel bundle in a used fuel container and $D_{g,1}$ is the gamma dose rate in water for a single fuel bundle in a pool of water. For the reference (324-bundle) used fuel copper container, Garisto et al. (2004) estimated F to be in the range 3 to 4.

3. ALPHA RADIATION DOSE RATES

Alpha decay is a nuclear decay in which a nucleus emits an alpha particle. An alpha particle consists of two protons and two neutrons (a helium nucleus). Thus an alpha particle may be represented either by the symbol α or He^{++}. Alpha decay is far more common in actinides and their decay products than in fission products or light elements. However, as noted above, the actinide decay chains also include beta decays.

3.1 METHODOLOGY AND ASSUMPTIONS

The total alpha dose rate is determined in accordance with the procedure described in Garisto et al. (2004), which is based on the methodology of Sunder (1995, 1998). In this approach, the time-dependent alpha dose rate in water, $D_\alpha(t)$, is given as a multiple of the time-dependent alpha dose rate in the fuel, $D_{\alpha,fuel}(t)$, based on the relative stopping power of alpha particles in water relative to uranium dioxide, Λ_α, and a factor of one-half to account for irradiation of the water from one side only, i.e.,

$$D_\alpha(t) = \Lambda_\alpha D_{\alpha,fuel}(t) / 2 \qquad (3.1)$$

The alpha dose rate in fuel, $D_{\alpha,fuel}(t)$ (in Gy/a or J/(a•kgUO_2)), is calculated at a location deep enough into the fuel so that all of the alpha energy is transferred to the fuel. The alpha dose rate in fuel is related to alpha power of the fuel, $H_{\alpha,fuel}(t)$ (in W/kgU), by Equation 3.2

$$D_{\alpha,fuel}(t) = (238/270)\ (3.156\text{x}10^7)\ H_{\alpha,fuel}(t) \qquad (3.2)$$

where the factor (238/270) converts kgU to kgUO_2 and the factor $3.156\text{x}10^7$ converts 1/s to 1/a. $H_{\alpha,fuel}(t)$ can be calculated directly from the known radionuclide inventories of the fuel and the radionuclide properties from Kocher (1981). Specifically,

$$H_{\alpha,fuel}(t) = \Sigma_j\ f_{\alpha j}\ H_{act,j}(t) \qquad (3.3)$$

where the sum is over all the radionuclides j in the fuel, $f_{\alpha j}$ is the fraction of the decay energy of radionuclide j that is alpha energy and $H_{act,j}(t)$ is the total decay power (W/kgU) of the jth radionuclide in the used fuel.

Equations 3.1 to 3.3 can be combined to give

$$D_\alpha(t) = 1.391\text{x}10^7\ \Lambda_\alpha\ \Sigma_j\ f_{\alpha j}\ H_{act,j}(t) \qquad (3.4)$$

3.2 ALPHA PARTICLE STOPPING POWER

In the Third Case Study (Garisto et al. 2004), a value of 1.39 was applied for Λ_α, the relative mass stopping power of alpha particles in water relative to uranium dioxide. This value was derived by Sunder (1995, 1998) using the approximation:

$$\Lambda_\alpha = \frac{\left(\frac{Z}{A}\right)_{H_2O}}{\left(\frac{Z}{A}\right)_{UO_2}} = \frac{\left(\frac{10}{18}\right)}{\left(\frac{108}{270}\right)} = 1.39. \qquad (3.5)$$

In the current work, since there is additional information available on the energy spectrum of the emitted alpha particles, the energy dependence of the relative mass stopping power was investigated. The mass stopping power of uranium dioxide for alpha particles was taken from Nitzki and Matzke (1973). Making use of their formulae for calculating the linear energy transfer (-dE/dx), where E is the particle energy and x is the distance travelled, the linear energy transfer was determined as a function of initial alpha particle energy. The mass stopping power (-(1/ρ)(dE/dx), where ρ is the density of the material) was then determined for uranium dioxide at a density of 10.6 g/cm^3.

Data for the mass stopping power of alpha particles in water were taken from the output of the computer program ASTAR available on the NIST web site (Berger et al. 2000). The ASTAR program reproduces the stopping powers for helium ions tabulated in ICRU Report 49 (ICRU 1993). The mass stopping power in water is shown in Table 3.1 for alpha particle energies ranging from 1 MeV to 9 MeV.

The mass stopping power of water for alpha particles relative to that of uranium dioxide is tabulated in Table 3.1 to illustrate variation with alpha particle energy. These data differ significantly from the approximate value of 1.39 derived by Sunder (1995, 1998).

The approximation based on the relative Z/A values as used by Sunder (1995, 1998) is widely used for low-Z materials; however, Nitzki and Matzke (1973) warned of large uncertainties in the calculated values of stopping power when neglecting inner shell corrections and due to uncertainty in the ionization potential of compounds. In providing support for the validity of the simple approximation, Sunder selected a value of the mass stopping power of 5.3 MeV alpha particles in water that was the lowest among the sources of data he quoted, the range of which encompassed more than a 3-fold variation. His chosen value of 43 keV/μm (or 430 MeV•cm^2/g) at 5.3 MeV is about half the corresponding value obtained using the ASTAR program, as shown in Table 3.1.

Between 1 and 9 MeV, the range of the Nitzki and Matzke (1993) data, the relative mass stopping power, Λ_α, varies between 2.80 and 3.74. Most of the alpha particle emissions from used fuel are in the energy range 4 to 5 MeV, but before reaching the fuel surface the alpha particles are attenuated by passage through, on average, about one half of their range in uranium dioxide. The relative mass stopping power at an energy of around 2.5 MeV, a value of about 3.25, would thus be more appropriate for use in the current application.

Table 3.1: Stopping power for alpha particles in uranium dioxide and in water

Alpha Particle Energy (MeV)	Nitzki & Matzke Linear Energy Transfer in UO_2 (MeV/μm)	Nitzki & Matzke Mass Stopping Power in UO_2 (ρ=10.6 g/cm^3) (MeV•cm^2/g)	ASTAR Mass Stopping Power in Water (MeV•cm^2/g)	Relative Mass Stopping Power Λ_α
1.00	0.621	585.96	2193	3.743
1.25	0.587	554.12	2052	3.703
1.50	0.557	525.57	1898	3.611
1.75	0.530	499.81	1754	3.509
2.00	0.505	476.46	1625	3.411
2.25	0.483	455.20	1512	3.322
2.50	0.462	435.75	1415	3.247
2.75	0.443	417.89	1330	3.183
3.00	0.426	401.45	1257	3.131
3.50	0.394	372.15	1133	3.044
4.00	0.367	346.84	1035	2.984
4.50	0.344	324.75	953.5	2.936
5.00	0.324	305.31	885.5	2.900
5.50	0.305	288.06	827.5	2.873
6.00	0.289	272.66	777.7	2.852
6.50	0.274	258.82	734.0	2.836
7.00	0.261	246.32	695.4	2.823
7.50	0.249	234.97	661.2	2.814
8.00	0.238	224.62	630.6	2.807
8.50	0.228	215.14	603.0	2.803
9.00	0.219	206.43	578.0	2.800

3.3 ALPHA DOSE RATES IN WATER AT THE FUEL SURFACE

The alpha dose rates in water in contact with the used fuel surface were calculated using Equation (3.4) with Λ_α = 3.25. The results of these calculations for three burnups are shown in Table 3.2. Table 3.3 shows the contributions of the actinides, fission products and light elements to the total alpha dose rate for used fuel with a burnup of 220 MWh/kgU. The contribution from the actinides is much larger than the contributions from either the fission products or light elements.

Table 3.2: Alpha dose rate in water (Gy/a) at fuel surface for various fuel burnups

Decay Time (years)	220 MWh/kgU	280 MWh/kgU	320 MWh/kgU
10	1.42E+06	1.94E+06	2.34E+06
20	1.72E+06	2.31E+06	2.74E+06
30	1.89E+06	2.52E+06	2.96E+06
40	1.99E+06	2.63E+06	3.07E+06
50	2.03E+06	2.68E+06	3.11E+06
60	2.05E+06	2.69E+06	3.12E+06
75	2.04E+06	2.67E+06	3.09E+06
100	2.00E+06	2.60E+06	3.00E+06
150	1.88E+06	2.43E+06	2.79E+06
200	1.77E+06	2.28E+06	2.61E+06
300	1.58E+06	2.02E+06	2.30E+06
500	1.30E+06	1.65E+06	1.86E+06
1000	9.03E+05	1.11E+06	1.24E+06
10^4	3.21E+05	3.67E+05	3.91E+05
10^5	1.80E+04	1.93E+04	2.00E+04
10^5	6.24E+03	6.97E+03	7.46E+03
10^7	4.19E+03	4.22E+03	4.24E+03

Table 3.3: Components of alpha dose rate in water at fuel surface (Gy/a) for a burnup of 220 MWh/kgU

Decay Time (years)	Total	Actinides	Fission Products	Light Elements
10	1.42E+06	1.42E+06	1.29E-03	8.69E-04
20	1.72E+06	1.72E+06	1.37E-03	8.20E-04
30	1.89E+06	1.89E+06	1.37E-03	8.20E-04
40	1.99E+06	1.99E+06	1.37E-03	8.20E-04
50	2.03E+06	2.03E+06	1.37E-03	8.20E-04
60	2.05E+06	2.05E+06	1.37E-03	8.20E-04
75	2.04E+06	2.04E+06	1.37E-03	8.20E-04
100	2.00E+06	2.00E+06	1.37E-03	8.20E-04
150	1.88E+06	1.88E+06	1.37E-03	8.20E-04
200	1.77E+06	1.77E+06	1.37E-03	8.20E-04
300	1.58E+06	1.58E+06	1.37E-03	8.19E-04
500	1.30E+06	1.30E+06	1.37E-03	8.19E-04
1000	9.03E+05	9.03E+05	1.37E-03	8.19E-04
10^4	3.21E+05	3.21E+05	1.37E-03	8.17E-04
10^5	1.80E+04	1.80E+04	1.37E-03	8.01E-04
10^5	6.24E+03	6.24E+03	1.37E-03	6.50E-04
10^7	4.19E+03	4.19E+03	1.37E-03	8.17E-05

3.4 ALPHA ENERGY FLUX AT THE FUEL SURFACE

The alpha particle energy flux at the surface of the fuel can be calculated using the stopping power data of Nitzki and Matzke (1973) and the results of Garisto (1989). Garisto had calculated that ¼ of alpha particles emitted within the range of the surface escaped from the fuel. The factor of ¼ is the exact results of a double integration of alpha particle emission from a uniform source in a semi-infinite planar medium.

Garisto also calculated that about 1/7th (with some dependence on decay time and burnup) of the alpha particle energy generated within the range R ($R \approx 11$ μm for 5.2 MeV alpha particles) of the fuel surface is emitted from the surface. The remaining energy is deposited within the fuel. This result was confirmed by a double integration performed numerically at different initial energies. The fraction of energy escaping from the surface depends slightly on the initial alpha particle energy. Thus, it seems reasonable that the dependence on burnup and decay time reported by Garisto is actually a function of the alpha particle energy spectrum, which is itself a function of power history, burnup and decay time.

The alpha energy generated per unit mass of uranium, $E_{gen/kgU}$, is the sum, over all the alpha emitting nuclides k, of the activity per unit mass of uranium (A_k) times the net alpha energy emitted per decay of nuclide k.. The net alpha energy emitted, in turn, is given by the sum over all transitions (j) for nuclide k of the probability of the transition per decay ($p_{i,j}$) times the energy ($E_{i,j}$) of the associated alpha particle, i.e.,

$$E_{gen/kgU} = \Sigma_k \{ A_k \Sigma_j [p_{k,j} E_{k,j}] \} \quad (3.6)$$

Alpha particles of energy E have a range R(E) in uranium dioxide. The mass per unit area of uranium within the range R(E) of the surface of a semi-infinite plane, $M_{U(E)/m2}$, is given by

$$M_{U(E)/m2} = \rho R(E) \times (AW_U/MW_{UO2}) \quad (3.7)$$

where ρ is the density of uranium dioxide, AW_U is the atomic weight of uranium and MW_{UO2} is the molecular weight of uranium dioxide. Thus, the total alpha energy per unit area of the fuel, $E_{gen,Ekj/m2}$, arising from the formation of alpha particles of energy $E_{k,j}$, within the range $R(E_{k,j})$ of the fuel surface, is given by

$$E_{gen,Ekj/m2} = \rho(AW_U/MW_{UO2}) A_k p_{k,j} E_{k,j} R(E_{k,j}) \quad (3.8)$$

Summing Equation 3.8 over all the radionuclides k and transitions j, one obtains the total alpha particle energy per unit area, $E_{gen/m2}$, generated within the range of the alpha particles to the surface, i.e.,

$$E_{gen,Ekj/m2} = \rho(AW_U/MW_{UO2}) \Sigma_k \{ A_k \Sigma_j [p_{k,j} E_{k,j} R(E_{k,j})] \} \quad (3.9)$$

Using the factor 1/7 for the energy escaping to the surface, the alpha energy flux escaping the surface, $E_{esc/m2}$, is

$$E_{esc/m2} = (\rho/7) (AW_U/MW_{UO2}) \Sigma_k \{ A_k \Sigma_j [p_{k,j} E_{k,j} R(E_{k,j})] \} \quad (3.10)$$

The range R of the alpha particles was calculated as a function of the alpha particle energy E using the relationship

$$R(E) = 0.5\ A\ E^2 + B\ E \qquad (3.11)$$

given by Nitzki and Matzke (1973). The constants A and B in the formula, as derived by Garisto (1989), are A = 0.37 μm•MeV^{-2} and B = 1.24 μm•MeV^{-1}. These values were used also to calculate the alpha linear energy transfer factors (-dE/dx) shown in Table 3.1 for uranium dioxide.

The same factor of 1/7 was applied for all values of $E_{k,j}$, as the variability with energy demonstrated in the numerical integration process amounted to no more than a few percent. The calculated results in MeV•μm•m^{-3}•s^{-1}, or equivalently eV•m^{-2}•s^{-1}, were converted to W/m^2. The resulting alpha energy fluxes at the fuel surface are tabulated in Table 3.4.

Table 3.4: Alpha energy fluxes (W/m^2) at the fuel surface for various burnup fuels

Decay Time (years)	220 MWh/kgU	280 MWh/kgU	320 MWh/kgU
10	4.91E-04	6.77E-04	8.23E-04
20	5.98E-04	8.09E-04	9.63E-04
30	6.59E-04	8.82E-04	1.04E-03
40	6.93E-04	9.20E-04	1.08E-03
50	7.09E-04	9.37E-04	1.09E-03
60	7.15E-04	9.41E-04	1.09E-03
75	7.12E-04	9.35E-04	1.08E-03
100	6.96E-04	9.09E-04	1.05E-03
150	6.54E-04	8.49E-04	9.75E-04
200	6.14E-04	7.94E-04	9.09E-04
300	5.47E-04	7.00E-04	8.01E-04
500	4.48E-04	5.68E-04	6.43E-04
1000	3.05E-04	3.78E-04	4.21E-04
10^4	1.05E-04	1.20E-04	1.28E-04
10^5	6.15E-06	6.59E-06	6.85E-06
10^5	2.45E-06	2.76E-06	2.97E-06
10^7	1.56E-06	1.57E-06	1.58E-06

Garisto (1989) reported values of alpha energy flux at the fuel surface for a few combinations of burnup and decay time. His results are tabulated in Table 3.5. The results of the current work at the nearest burnup are provided for comparison. As can be seen from the table, the values of the alpha energy flux out of the fuel surface calculated in this report agree reasonably well with those of Garisto (1989), particularly if allowance is made for the differences in burnup.

Table 3.5: Comparison of calculated alpha energy fluxes at fuel surface

Decay Time (years)	Energy Flux Out (MeV/cm^2/s)	
	Garisto (1989)	This Work
100	3.44E+05 at 685 GJ/kgU	4.34E+05 at 792 GJ/kgU
1000	1.63E+05 at 685 GJ/kgU	1.91E+05 at 792 GJ/kgU
10000	6.16E+04 at 685 GJ/kgU	6.57E+04 at 792 GJ/kgU
1000	2.43E+05 at 1045 GJ/kgU	2.36E+05 at 1008 GJ/kgU

4. BETA DECAY

Beta decay occurs when a nucleus emits a beta particle (an electron). Beta decay is often, but not always, accompanied by gamma emission. Most of the fission products and light elements are beta-gamma emitters. However, some of the actinides and their decay products are also beta emitters. In the Third Case Study, the approximation was made that the beta decay energy is the difference between the total decay energy and gamma decay energy for fission products and light elements. However, in the current work, beta decay power fractions were calculated on a nuclide-by-nuclide basis, similarly to what done in Section 3 for alpha decay.

4.1 BETA PARTICLE STOPPING POWER

Sunder (1995, 1998) provided a tabulation of beta particle stopping powers for water and for uranium dioxide. From this table, Garisto et al. (2004) calculated the relative stopping power of beta particles in water relative to uranium dioxide, Λ_β. They found Λ_β = 1.8 for beta particles with an energy of 0.3 MeV.

Equivalent information was obtained from the output of the computer program ESTAR available on the NIST web site (2000). The ESTAR program generates stopping powers and ranges for electrons which are the same as those tabulated in ICRU Report 37 (ICRU 1984). Both liquid water and uranium dioxide are available in ESTAR as standard materials, although the program can calculate similar tables for any other element, compound or mixture. The value of Λ_β decreases from 2.09 to 1.42 as the beta particle energy increases from 0.05 MeV to 2.3 MeV.

The ESTAR data for mass stopping power of water is essentially identical to that provided by Sunder (1995, 1998), since both are taken directly from ICRU Report 37. Sunder's values for uranium dioxide, which were calculated from the elemental values using an additivity law, differ from the ESTAR data by no more than a few percent. Hence, any change in the relative mass stopping power at a given beta particle energy arising from use of the alternative source of data would be insufficient to justify an update to the value of 1.8 previously selected by Garisto et al. (2004) as representative of the relative mass stopping power over the relevant range of beta energies.

4.2 BETA DOSE RATES IN WATER AT THE FUEL SURFACE

The calculation of beta dose rate is similar to that of alpha dose rate (Section 3.1) and the variables below have analogous definitions. In this approach, the beta dose rate in water, D_β (in Gy/a or J/(a•kgUO_2)), is expressed in terms of the beta dose rate in the fuel, $D_{\beta,fuel}$, i.e.,

$$D_\beta(t) = \Lambda_\beta \, D_{\beta,fuel}(t) / 2 \qquad (4.1)$$

where Λ_β is the relative mass stopping power for beta particles in water relative of uranium dioxide. The beta dose rate deep in the fuel can be calculated from the beta power of the fuel, $H_{\beta,fuel}(t)$ (in W/kgU), using the equation

$$D_{\beta,fuel}(t) = (238/270) \, (3.156 \times 10^7) \, H_{\beta,fuel}(t) \qquad (4.2)$$

The value of $H_{\beta,fuel}(t)$ can be calculated on a nuclide by nuclide basis, i.e.,

$$H_{\beta,fuel}(t) = \Sigma_j \, f_{\beta j} \, H_{act,j}(t) \qquad (4.3)$$

where the sum is over all the radionuclides in the fuel, $f_{\beta j}$ is the fraction of the decay energy of radionuclide j that is beta energy and $H_{act,j}(t)$ is the total decay power (W/kgU) of the jth radionuclide in used fuel. Combining Equations 4.1 to 4.3 and using Λ_β = 1.8, gives

$$D_\beta(t) = 2.504 \times 10^7 \, \Sigma_j \, f_{\beta j} \, H_{act,j}(t) \qquad (4.4)$$

The beta dose rates at the fuel surface calculated with Equation 4.4 are shown in Table 4.1.

The contributions of the actinides, fission products and light elements to the beta dose rates at the fuel surface are given in Table 4.2 for used fuel with a burnup of 220 MWh/kgU. They are also shown in Figure 4.1. At decay times up to about 200 years, the beta dose rate is primarily that from fission product decay with the actinide decay products contributing only a small fraction to the total beta dose rate. However, at longer decay times, most of the fission products have decayed leaving the actinide decay products as the primary source of the beta dose rate (see Figure 4.1). However, at these long times, the beta dose rate is much smaller than the alpha dose rate (cf. Tables 3.2 and 4.1).

In Garisto et al. (2004), the approximation was made that the beta decay energy is equal to the difference between the total decay energy and gamma energy from fission products and light elements. This neglected the beta energy from the actinides. As shown in Table 4.2, this is a poor approximation at decay times greater than about 200 years. However, at decay times greater than about 200 years, alpha doses rates are much larger than beta dose rates so that this approximation would not have introduced a significant error in the fuel dissolution rates calculated in the Third Case Study (Garisto et al. 2004).

Table 4.1: Beta dose rates (Gy/a) in water at the fuel surface for various burnup fuels

Decay Time (years)	220 MWh/kgU	280 MWh/kgU	320 MWh/kgU
10	3.77E+06	4.56E+06	5.06E+06
20	2.82E+06	3.41E+06	3.79E+06
30	2.20E+06	2.66E+06	2.95E+06
40	1.72E+06	2.08E+06	2.31E+06
50	1.35E+06	1.63E+06	1.81E+06
60	1.06E+06	1.28E+06	1.42E+06
75	7.38E+05	8.92E+05	9.90E+05
100	4.04E+05	4.90E+05	5.44E+05
150	1.24E+05	1.50E+05	1.67E+05
200	3.96E+04	4.85E+04	5.41E+04
300	6.66E+03	8.48E+03	9.67E+03
500	2.69E+03	3.56E+03	4.15E+03
1000	1.53E+03	2.01E+03	2.34E+03
10^4	3.78E+02	4.66E+02	5.29E+02
10^5	1.68E+02	1.91E+02	2.06E+02
10^6	1.49E+02	1.59E+02	1.66E+02
10^7	1.15E+02	1.15E+02	1.15E+02

Table 4.2: Components of the beta dose rates in water at the fuel surface (Gy/a) for fuel with a burnup of 220 MWh/kgU

Decay Time (years)	Total	Actinides	Fission Products	Light Elements
10	3.77E+06	1.67E+04	3.74E+06	7.48E+03
20	2.82E+06	1.22E+04	2.81E+06	2.08E+03
30	2.20E+06	9.41E+03	2.19E+06	6.03E+02
40	1.72E+06	7.64E+03	1.72E+06	1.91E+02
50	1.35E+06	6.52E+03	1.35E+06	7.13E+01
60	1.06E+06	5.80E+03	1.05E+06	3.44E+01
75	7.38E+05	5.16E+03	7.32E+05	1.86E+01
100	4.04E+05	4.63E+03	4.00E+05	1.27E+01
150	1.24E+05	4.17E+03	1.19E+05	9.78E+00
200	3.96E+04	3.87E+03	3.57E+04	8.27E+00
300	6.66E+03	3.36E+03	3.29E+03	6.36E+00
500	2.69E+03	2.58E+03	1.08E+02	4.61E+00
1000	1.53E+03	1.45E+03	7.77E+01	3.46E+00
10^4	3.78E+02	3.02E+02	7.45E+01	1.42E+00
10^5	1.68E+02	1.17E+02	5.09E+01	3.58E-01
10^6	1.49E+02	1.45E+02	3.71E+00	4.30E-01
10^7	1.15E+02	1.15E+02	1.09E-01	6.35E-05

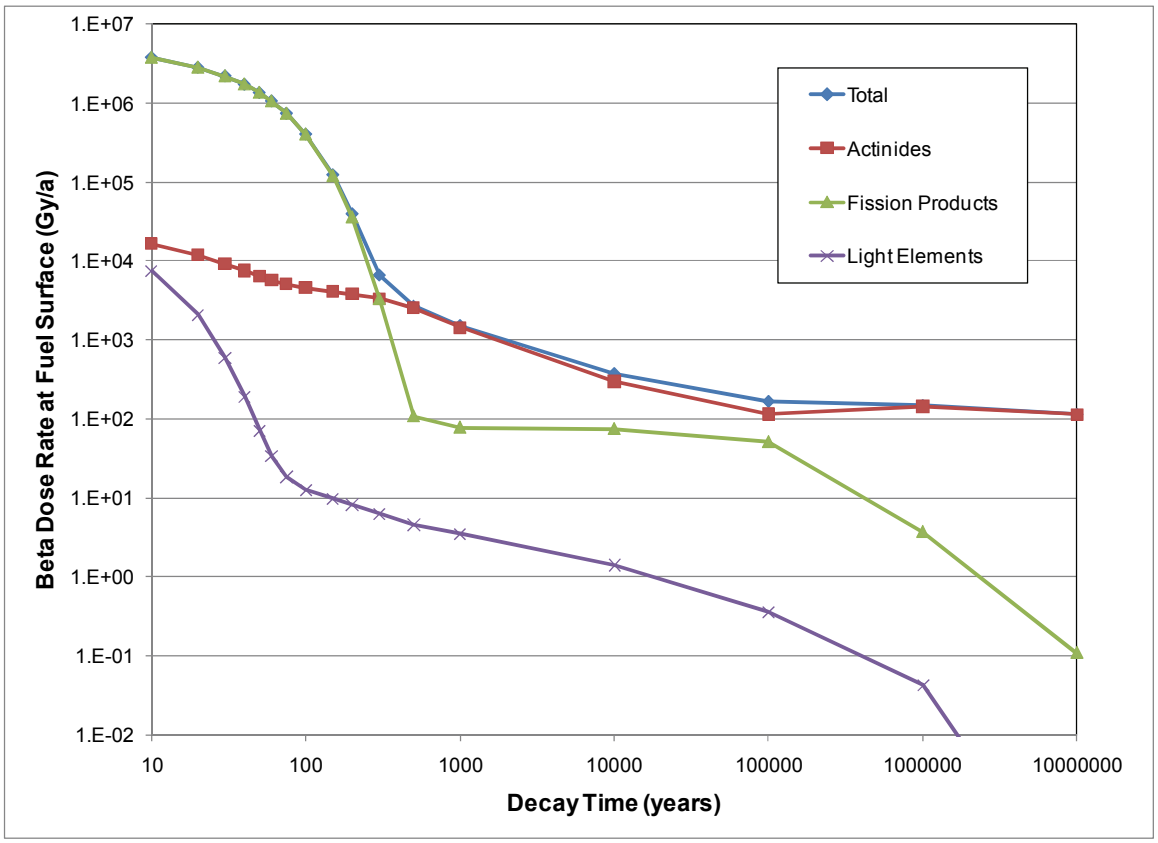

Figure 4.1: Components of the beta dose rate at the fuel surface.

4.3 BETA DOSE RATE At 50 µm INTO THE WATER LAYER

The average energy of beta radiation from fuel decayed for more than 10 years is calculated to be 0.3 MeV using the data in Tait and Hanna (2001). To account for passage of some of this radiation through the fuel prior to reaching its surface, an average energy for beta particles leaving the fuel surface can be assumed to be about half this amount (≈ 0.15 MeV). At this reduced energy, the range of the beta particles entering the water is on the order of 280 µm. The mass stopping power for water at a beta energy of 0.15 MeV is about 3.2 MeV•cm^2•g^{-1}, based on the data tabulated by Sunder (1995, 1998). This stopping power corresponds to a loss of about 0.016 MeV (about 10%) of the beta particle energy in a 50 µm path.

This result indicates that beta dose rates at a depth of 50 µm into the water layer would likely not be greatly different from dose rates at the fuel surface. More detailed calculations to represent the geometry and energy distribution of the source using energy dependent stopping powers are needed to refine this conclusion. It is possible that greater attenuation would be calculated for the more diffuse source associated with a fuel element rather than for a narrow beam geometry.

5. GAMMA RADIATION DOSE RATE

In this section, the gamma radiation dose rate near a used fuel bundle in a water filled reference copper shelled IV-324-HEX used fuel container (Maak and Simmons 2001) is calculated. The calculations are divided into two main parts:

1. The gamma radiation dose rate from a single Bruce 37-element fuel bundle in an infinite pool of water is calculated. The objective of this part is to calculate average gamma dose rates in water within the bundle envelope.
2. The gamma radiation dose rates within bundle envelopes in various parts of the IV-324-HEX used fuel container are calculated.

The main objective of these calculations is to determine the gamma dose rates near a fuel bundle within the flooded used fuel container as well as the F factor, which represents the relative contribution of the surrounding fuel bundles to the gamma radiation dose rate near a particular fuel bundle in the used fuel container.

5.1 METHODOLOGY AND ASSUMPTIONS

All gamma dose calculations were carried out using the Monte Carlo N-Particle (MCNP) software, version 5.1.3 (X-5 Monte Carlo Team 2003). MCNP is capable of simulating transport of neutrons, photons and electrons. Unlike most other radiation transport codes, MCNP does not resort to the numerical solution of the Boltzmann transport equation (or an approximation thereof); instead, using a Monte Carlo technique based on the interaction probability distributions for each event, the code simulates interaction of particles/photons with matter by following the tracks of each particle/photon generated within a specified source.

The gamma photon spectra, as a function of decay time (i.e., time after discharge of the fuel from the reactor), were extracted from Tait et al. (2000). Each spectrum is divided into 18 discrete energy groups, where the lowest and highest mean energies are 0.01 MeV and 5.50 MeV, respectively. Energy ranges and the corresponding mean energies of the 18 energy groups are shown in Table 5.1 below.

Fuel burnup was not inherently reflected in the MCNP simulations; instead it was accounted for during data post-processing. That is, the model for each particular case was executed separately for each of the 18 energy groups. Subsequently, the results were prorated and combined to reflect the gamma photon spectra for specific decay times and fuel burnups as given in Tait et al. (2000). All results presented in this work, unless explicitly specified, assume a fuel burnup of 220 MWh/kgU.

The total number of photons generated within each fuel element was dependent on the specific case and energy group, and was adjusted so as to provide satisfactory statistical validity of each quantity being tallied. The target criterion was an estimated standard deviation of a fraction of a percent.

Material compositions for all materials used in this project are shown in Appendix A.

Table 5.1: Discrete energy groups used to specify photon spectra for the various fuel burnups in Tait et al. (2000)

Mean Photon Energy (MeV)	Energy Range (MeV)		
0.010	0	-	0.02
0.030	0.02	-	0.04
0.055	0.04	-	0.07
0.085	0.07	-	0.1
0.120	0.1	-	0.14
0.170	0.14	-	0.2
0.300	0.2	-	0.4
0.650	0.4	-	0.9
1.120	0.9	-	1.34
1.580	1.34	-	1.82
2.000	1.82	-	2.18
2.400	2.18	-	2.62
2.800	2.62	-	2.98
3.250	2.98	-	3.52
3.750	3.52	-	3.98
4.250	3.98	-	4.52
4.750	4.52	-	4.98
5.500	4.98	-	6.02

General assumptions applied to all calculations are as follows:

1. Dimensions of a standard Bruce 37-element fuel bundle were assumed.

2. Zircaloy bundle end plates, bearing pads and spacers were not modeled, unless otherwise stated.

3. The temperature of water surrounding a bundle, and hence its density, is subject to variation as a function of decay time. The expected temperature range is approximately 15^{o}C to 95^{o}C (McMurry et al. 2003). However, instead of employing a different water density for each decay time, a value corresponding to the temperature of 55^{o}C was used. At 55^{o}C and a pressure of 5 MPa the density of water is 0.9878 g/cm^{3}. Sensitivity calculations were performed to study the impact of temperature on the calculated gamma dose rates.

4. The distribution of gamma photons emitted within a single element in the axial direction was uniform (flat). In the radial direction, however, the distribution of gamma photons was biased towards the element centreline. This assumption is somewhat non-conservative in this application. Thus, a sensitivity analysis was carried out to determine the sensitivity of the calculated gamma dose rates on the distribution of gamma photons emitted in the radial direction.

5. Used fuel was assumed to occupy the entire space within the cladding – i.e., the air gap between the fuel and fuel sheath was not modelled. As such, the mass of fuel material per unit length of a fuel element was overestimated by 0.5%.

6. The densities of used fuel and the Zircaloy cladding were set to 10.515 g/cm^3 and 6.39 g/cm^3, respectively.

7. The chemical composition of used fuel corresponded to burnup of 220 MWh/kgU, unless otherwise mentioned. The presence of americium isotopes was excluded as the photon cross-sections for this element are not present in the MCNP cross-section library. Since the total mass of Am isotopes amounts to less than 0.1% of bundle fuel mass, the density of the remaining nuclides was renormalized so as to conserve the nominal density of the UO_2 matrix, namely, 10.515 g/cm^3.

Further assumptions pertaining to each specific model are listed in the respective sections below.

5.2 FUEL BUNDLE IN AN INFINITE POOL OF WATER

In this section, the gamma dose rate from an isolated used fuel bundle in an infinite pool of water is calculated. For the nominal case, a single Bruce 37-element bundle was placed at the centre of a large water-filled sphere. The density of water was set to 0.9878 g/cm^3, i.e., that corresponding to a temperature of 55^{o}C and a pressure of 5 MPa.

Dose rates, that is, average gamma energy deposition per unit mass and unit time, in water within the bundle envelope were calculated based on a fuel burnup of 220 MWh/kgU. Measured from the bundle centre, the radius of the bundle envelope was defined at 4.982 cm; in comparison, the Zircaloy cladding in any element located in the outermost fuel ring extends to a radius of 4.980 cm. Average gamma energy deposition in the fuel elements and Zircaloy cladding were also calculated.

In addition to the nominal case, a number of sensitivity calculations were carried out; these are as follows:

- Water Density - Impact of the change in water density was assessed by adjusting the density to two bounding values, 0.9999 g/cm^3 and 0.9650 g/cm^3, corresponding to temperatures of approximately 0^{o}C and 90^{o}C, respectively.
- Zircaloy Cladding - In order to assess the importance of the Zircaloy cladding in shielding the gamma radiation generated in the used fuel, a sensitivity case without the Zircaloy cladding was investigated.
- Bundle Envelope Size - The radius of the bundle envelope was defined to approximately coincide with the outer edge of fuel sheaths on the periphery of a bundle. The definition of this bundle envelope differs from that in Section 5.3, where its radius coincides with that of the inner radius of the carbon steel tubes furnishing the IV-324-HEX container. As such, a sensitivity case was executed to determine the sensitivity of the average gamma energy deposited in water within the bundle envelope to the change in the size of the bundle envelope.
- Radial Distribution of Gamma Photons - Sensitivity of the energy deposited in water within the bundle envelope to the nature of the radial gamma photon distribution within the fuel elements was investigated.
- Fuel Burnup - Sensitivity to fuel burnup was assessed by prorating the results from the nominal case (with burnup of 220 MWh/kgU) to photon spectra corresponding to fuel burnups of 280 MWh/kgU and 320 MWh/kgU.

Uncertainties in dose rates in water within the bundle envelope were assessed based on the standard deviation in energies from the MCNP simulations (referred to as statistical uncertainty in the remainder of this document) as well as a representative uncertainty attributed to the gamma photon spectra.

Further to the assumptions stated in Section 5.1, the following assumption was invoked for the current case:

- Zircaloy plugs located at both ends of each fuel element were not modelled. The entire length of each element (and thus the total height of a UO_2 stack) was 49.53 cm.

5.2.1 Results: Nominal Case

As previously described, the nominal case assumes a water density of 0.9878 g/cm^3, a fuel burnup of 220 MWh/kgU and the Zircaloy cladding fully intact. The total mass of water within the bundle envelope is 1.4 kg.

Table 5.2 shows the relative distribution of total gamma energy deposited within the system, as a function of decay time, among all the components of the system; namely, fuel material, Zircaloy cladding and water inside and outside of the bundle envelope.

Generally, about 80% of the gamma photon energy from used fuel is absorbed within the UO_2 fuel matrix itself. At decay times of 500 and 1000 years the fraction of energy deposited in fuel material increases up to about 99%. Subsequently, at 10^4 to 10^5 years, this fraction reverts to the range characteristic of the previous decay times, and at longer times it decreases to about 75%. This behaviour is a reflection of the shape of the used fuel gamma photon spectra.

Absorption of a large fraction of total gamma energy within the fuel material means that the gamma spectrum, at the particular decay time, is dominated mostly by gamma photons with low energies. Conversely, when this fraction is smaller, it means a greater intensity of photons with energies high enough to penetrate fuel elements is present. Figure 5.1 shows the gamma photon spectra for the discrete energy groups with mean energies ranging from 0.12 MeV to 3.25 MeV - i.e., those accounting for the bulk of the total gamma energy - as a function of decay time. Photon group energy boundaries for these mean energies are shown in Table 5.1.

All the energy groups shown in Figure 5.1 undergo a clear intensity decrease in the decay time range of 500 to 1000 years. Following the decay time of 1000 years, however, the intensity of the gamma energy groups with mean energies above 1 MeV can be seen to increase with increasing decay time (as a result of the radionuclide ingrowth). In fact, for some energy groups this increase spans as much as three orders of magnitude. This increase in the high energy photon intensity corresponds to the decrease in the fraction of total energy absorbed in used fuel.

Table 5.2 also indicates that up to 2% of the total energy is absorbed within the Zircaloy cladding. For most decay times, the energy fraction deposited in the water within the fuel envelope is in the range 1.2 to 1.7%. The remaining fraction of the total energy, amounting to about 10% to 20%, escapes outside of the surface defining the bundle envelope.

Table 5.2: Fractional distribution of absorbed gamma energy, within the various components of the system, as a function of decay time – nominal case.

Body:	Fraction of Total Energy as a Function of Decay Time (years)									
	10 yr.	50 yr.	100 yr.	200 yr.	500 yr.	10^3 yr.	10^4 yr.	10^5 yr.	10^6 yr.	10^7 yr.
Fuel Elements	82.4%	83.6%	83.7%	84.9%	99.1%	98.8%	91.0%	80.6%	76.6%	74.3%
Cladding	2.0%	1.9%	1.9%	1.8%	0.2%	0.2%	1.1%	1.9%	2.1%	2.2%
Water Inside Bundle Envelope	1.3%	1.3%	1.3%	1.2%	0.1%	0.1%	0.7%	1.3%	1.6%	1.7%
Water Outside of Bundle Envelope	14.3%	13.2%	13.1%	12.1%	0.7%	0.9%	7.2%	16.2%	19.8%	21.7%

Table 5.3 presents the average dose rates within the Zircaloy cladding and the water inside the bundle envelope as a function of decay time. As can be expected from the data presented in Table 5.2, dose rates in both bodies are similar. The increase in the gamma dose rates to water between the decay times 1000 and 10^6 years corresponds to the increase in the intensity of the gamma photons with energies above 1 MeV depicted in Figure 5.1. Such high energy photons escape from the fuel matrix more readily than low energy photons, and thus a higher fraction of their energy is deposited in water within the fuel envelope.

Table 5.3: Average gamma dose rates in Zircaloy cladding and water inside fuel envelope, as a function of decay time - nominal case.

Body:	Dose Rates (Gy/hr) as Function of Decay Time (years)									
	10 yr.	50 yr.	100 yr.	200 yr.	500 yr.	10^3 yr.	10^4 yr.	10^5 yr.	10^6 yr.	10^7 yr.
Cladding	8.11E+1	2.61E+1	8.15E+0	8.10E-1	4.75E-3	2.92E-3	2.06E-3	2.86E-3	3.56E-3	3.24E-3
Water Inside Bundle Envelope	7.30E+1	2.29E+1	7.15E+0	7.07E-1	2.37E-3	1.62E-3	1.69E-3	2.71E-3	3.56E-3	3.30E-3

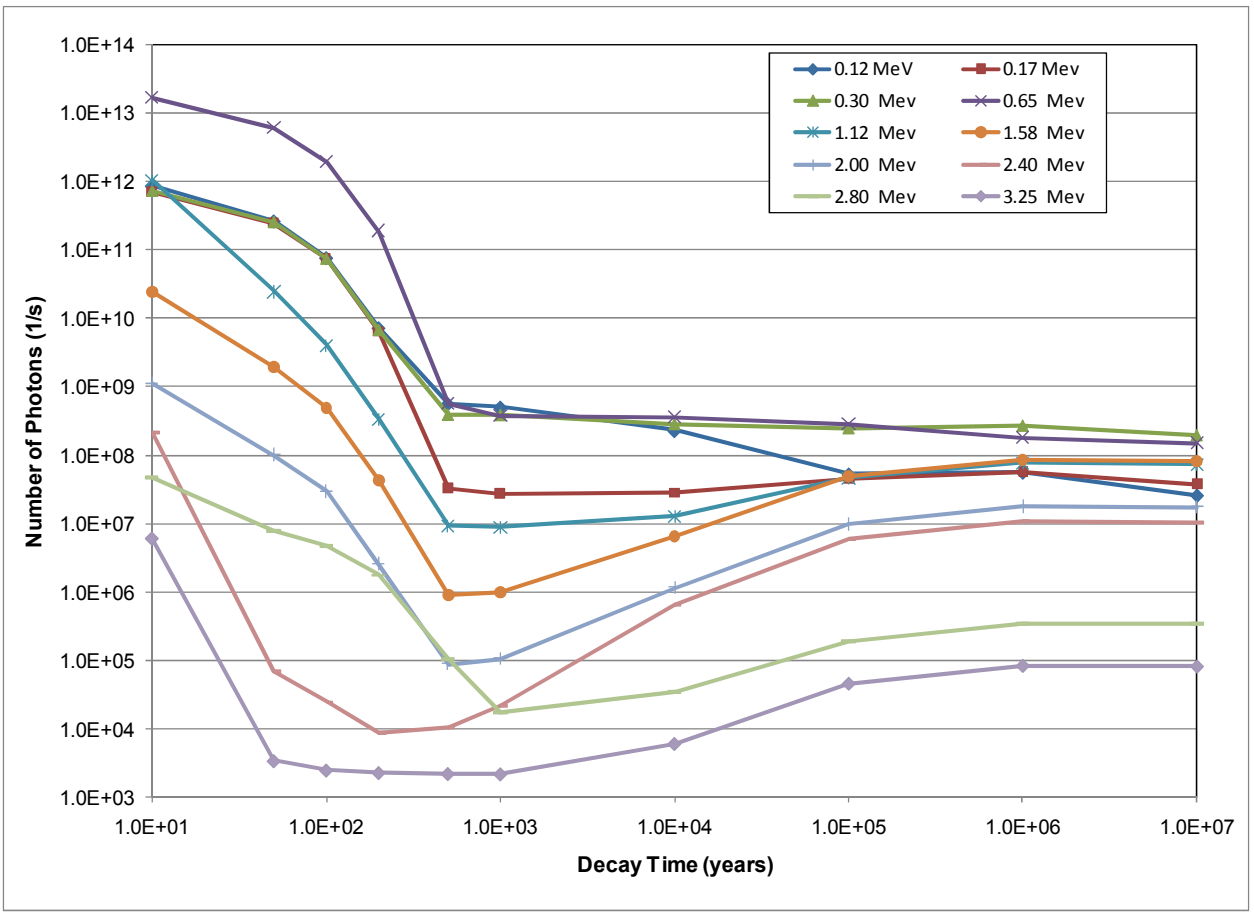

Figure 5.1: Gamma photon spectra for used fuel with a burnup of 220 MWh/kgU for discrete energy groups with mean gamma energies from 0.12 MeV to 3.25 MeV.

5.2.2 Impact of the Absence of Zircaloy Cladding

This section presents the results of a case analogous to that of the nominal scenario, except that the volume previously occupied by Zircaloy cladding has now been replaced by water. This change increases the total amount of water within the fuel bundle envelope from 1.4 kg to 1.7 kg.

The average dose rates in water within the bundle envelope in the absence of the cladding are compared to the dose rates in the nominal scenario in Tables 5.4 and 5.5. Table 5.4 presents the actual dose rates and Table 5.5 presents the variation in dose rate relative to the nominal scenario. Removal of the Zircaloy cladding increases the dose rates in the water within the bundle envelope by approximately 3%.

Table 5.4: Dose rates in water within the bundle envelope for the nominal case and the sensitivity cases

Case:	Dose Rates in Water within Bundle Envelope (Gy/hr) as Function of Decay Time									
	10 yr.	50 yr.	100 yr.	200 yr.	500 yr.	10^3 yr.	10^4 yr.	10^5 yr.	10^6 yr.	10^7 yr.
Nominal Case	7.30E+1	2.29E+1	7.15E+0	7.07E-1	2.37E-3	1.62E-3	1.69E-3	2.71E-3	3.56E-3	3.30E-3
Removed Cladding	7.51E+1	2.35E+1	7.35E+0	7.28E-1	2.50E-3	1.69E-3	1.74E-3	2.79E-3	3.66E-3	3.40E-3
Water Density: 0.9650 g/cm^3	7.30E+1	2.29E+1	7.15E+0	7.08E-1	2.38E-3	1.62E-3	1.69E-3	2.71E-3	3.56E-3	3.30E-3
Water Density: 0.9999 g/cm^3	7.29E+1	2.29E+1	7.14E+0	7.07E-1	2.37E-3	1.62E-3	1.69E-3	2.71E-3	3.56E-3	3.30E-3
Uniform Photon Distribution in the Radial Direction	7.71E+1	2.43E+1	7.58E+0	7.50E-1	2.56E-3	1.75E-3	1.80E-3	2.83E-3	3.70E-3	3.42E-3
Larger Bundle Envelope	6.52E+1	2.04E+1	6.38E+0	6.32E-1	2.12E-3	1.45E-3	1.51E-3	2.43E-3	3.20E-3	2.97E-3
Burnup: 280 MWh/kgU	9.39E+1	2.90E+1	9.03E+0	8.95E-1	3.21E-3	2.25E-3	2.23E-3	3.05E-3	3.61E-3	3.29E-3
Burnup: 320 MWh/kgU	1.08E+2	3.31E+1	1.03E+1	1.02E+0	3.82E-3	2.72E-3	2.61E-3	3.30E-3	3.65E-3	3.29E-3

5.2.3 Sensitivity to Change in Water Density

The temperature of the water surrounding a used fuel bundle, and hence its density, is subject to variation as a function of time. The expected temperature range is approximately 15°C to 90°C. In the nominal case, a midpoint temperature of 55°C was assumed, corresponding to a water density of 0.9878 g/cm^3 at a pressure of 5 MPa. In order to assess the sensitivity of the gamma energy deposited in water to a change in water density, two additional cases were evaluated. The water density in those cases was set to 0.9650 g/cm^3 and 0.9999 g/cm^3, corresponding to temperatures of about 90°C and 0°C, respectively.

The calculated dose rates in the water envelope for these two temperatures are compared to the corresponding dose rates in the nominal case in Table 5.4. The variation of these dose rates (in percentage) relative to the nominal case are shown in Table 5.5. The data in both tables clearly demonstrate that any differences due to change in water density within the inspected range are minimal, and in all cases are well below 1%.

Table 5.5: Variation in dose rates in water within the bundle envelope relative to the nominal case

Case:	Variation in Dose Rates in Water within Bundle Envelope (%)*									
	10 yr.	50 yr.	100 yr.	200 yr.	500 yr.	10^3 yr.	10^4 yr.	10^5 yr.	10^6 yr.	10^7 yr.
Removed Cladding	+2.9 %	+2.9 %	+2.9 %	+2.9 %	+5.2 %	+4.5 %	+3.0 %	+2.9 %	+2.9 %	+2.9 %
Water Density: 0.9650 g/cm^3	+0.07 %	+0.06 %	+0.06 %	+0.06 %	+0.06 %	+0.06 %	+0.06 %	+0.07 %	+0.07 %	+0.07 %
Water Density: 0.9999 g/cm^3	-0.04 %	-0.04 %	-0.04 %	-0.04 %	-0.04 %	-0.04 %	-0.04 %	-0.04 %	-0.04 %	-0.04 %
Uniform Photon Distribution in the Radial Direction	+5.6 %	+6.0 %	+6.0 %	+6.0 %	+7.9 %	+8.2 %	+8.2 %	+4.6 %	+3.8 %	+3.6 %
Larger Bundle Envelope	-11.9%	-12.0%	-12.0%	-12.0%	-11.9%	-11.9%	-11.8%	-11.4%	-11.2%	-11.2%
Burnup: 280 MWh/kgU	+28.7 %	+26.7 %	+26.3 %	+26.5 %	+35.3 %	+38.8 %	+32.0 %	+12.7 %	+1.5 %	-0.2 %
Burnup: 320 MWh/kgU	+48.5 %	+44.7 %	+44.5 %	+44.8 %	+60.7 %	+67.8 %	+54.7 %	+22.0 %	+2.7 %	-0.3 %

*A +/- sign indicates that the dose rate in the given case is higher/lower than for the nominal case.

5.2.4 Sensitivity to Radial Photon Distribution

In the nominal case, the distribution of gamma photons within fuel elements along the axial direction was assumed to be flat; whereas, in the radial direction, the gamma photon distribution was biased towards the fuel element centerline. This is a non-conservative assumption with respect to energy deposition in water. Thus, a sensitivity case with a more realistic radial distribution was investigated.

Table 5.6 below shows the fractional distribution of total deposited energy (per unit time) within fuel elements, cladding and water within the bundle envelope as a function of time after fuel discharge, for the case adopting a uniform distribution of gamma photons in the radial direction within fuel elements. The percentages in parenthesis indicate the change in the fractions in comparison to the nominal case with a centerline-biased radial distribution. The results in Table 5.6 indicates that assuming a flat radial distribution within fuel elements leads to less energy being deposited in fuel elements and, as a result, more energy being deposited in the cladding and water within the bundle envelope. For most decay times the fraction of total energy deposited in fuel elements decreases by (an absolute amount) of approximately 0.6-0.7%; the differences in the total energy deposition fractions in Zircaloy cladding and water within the bundle envelope are on the order of 0.1%.

The dose rates in water within the bundle envelope for the case with a uniform radial photon distribution within fuel elements are shown in Table 5.4 and the variations in the dose rates, relative to the nominal case, are shown in Table 5.5. At decay times less than 200 years, the dose rates increase by about 6%. At decay times characterized by the relatively soft spectra, that is, those ranging from about 500 to 10000 years, the increases are seen to be close to 8%, and finally at long decay times, dose rates increase by about 3.5 to 4.5%.

Table 5.6: Fractional distribution of total energy per unit time, within the various components of the system, as a function of time after fuel discharge – uniform radial photon distribution.

Body:	Fraction of Total Energy as a Function of Decay Time (years)									
	10 yr.	50 yr.	100 yr.	200 yr.	500 yr.	10^3 yr.	10^4 yr.	10^5 yr.	10^6 yr.	10^7 yr.
Fuel Elements	81.6% (-0.7%)*	82.8% (-0.7%)	83.0% (-0.7%)	84.2% (-0.7%)	99.0% (-0.1%)	98.6% (-0.1%)	90.5% (-0.5%)	79.9% (-0.6%)	76.0% (-0.6%)	73.7% (-0.6%)
Zircaloy Cladding	2.1% (+0.14%)	2.1% (+0.14%)	2.1% (+0.14%)	1.9% (+0.14%)	0.2% (+0.14%)	0.3% (+0.08%)	1.2% (+0.13%)	2.0% (+0.15%)	2.2% (+0.14%)	2.4% (+0.13%)
Water Inside Bundle Envelope	1.4% (+0.08%)	1.3% (+0.08%)	1.3% (+0.08%)	1.2% (+0.07%)	0.1% (+0.005%)	0.1% (+0.007%)	0.7% (+0.05%)	1.4% (+0.06%)	1.6% (+0.06%)	1.8% (+0.06%)

*Numbers in parenthesis indicate the absolute change in a given fraction in comparison to the corresponding value in Table 5.2, that is, the nominal case (with photon distribution biased towards fuel element centerline). A plus/minus sign indicates that the current percentage value is higher/lower.

5.2.5 Sensitivity to the Size of the Bundle Envelope

The radius of the bundle envelope in the nominal case was chosen so as to enclose the fuel entire bundle; as such its value was set to 4.982 cm. However, since the bundles in the IV-324-HEX used fuel container are physically confined to carbon steel tubes of inner radius 5.250 cm, this latter dimension has been used as the size of the bundle envelope in the subsequent calculations involving the fuel bundles as arranged in the used fuel container.

The F-factor (see Section 5.3.5) describes the ratio of dose rate in water within the bundle envelope for the case of multiple bundles (e.g., inside a used fuel container) relative to the dose rate in water within the bundle envelope for a single bundle in an infinite pool of water. Since the bundle envelope size must be consistent between the two cases, the energy deposition in water for the case of a single bundle in an infinite pool of water was also evaluated for the larger bundle envelope radius of 5.250 cm. The calculated dose rates for this case are shown in Table 5.4.

Since the energy deposited per unit mass of water decreases with increasing distance from the source (bundle), enlarging the bundle envelope radius from 4.982 cm to 5.250 cm will lower the average energy per unit mass deposited in water within the bundle envelope. Data in Table 5.4 confirms this expectation. In comparison to the nominal case, the dose rates in the current case are approximately 11 to 12% lower, as indicated in Table 5.5.

The calculated dose rates presented in this section will be employed for the evaluation of the F-factors in Section 5.3.

5.2.6 Sensitivity to Fuel Burnup

Dose rates calculated for the nominal case have been derived with the gamma photon spectra corresponding to fuel burnup of 220 MWh/kgU. In order to assess the sensitivity of average dose rates in the water within the bundle envelope to the extent of fuel burnup, the results of the nominal case have also been prorated to photon spectra corresponding to fuel burnups of 280 MWh/kgU and 320 MWh/kgU. The results corresponding to these sensitivity cases are shown in Table 5.4 and compared to those for the nominal case in Table 5.5.

For decay times less than about 10^4 years, calculated gamma dose rates within the bundle envelope for fuel burnups of 280 MWh/kgU and 320 MWh/kgU are, on average, about 30% and 50% higher, respectively, than those for a fuel burnup of 220 MWh/kgU. This difference is similar to the difference in the burnups (27% and 45%, respectively). However, at decay times longer than 10^4 years, the effect of higher burnup starts to diminish, and at 10^7 years, dose rates are essentially independent of burnup.

Further, comparison of the results from the nominal case with those corresponding to the two higher burnups showed that burnup dependent changes in photon spectra (at a given decay time) did not have a significant impact on the fractions of the total energy deposited among the various components of the system.

5.2.7 Sensitivity and Uncertainty Assessments

Table 5.7 shows the uncertainty estimates (one standard deviation) due to the MCNP modelling technique itself and the combined uncertainty due to the modelling technique and uncertainties

in the photon source spectra. All uncertainty propagation calculations have been carried out assuming there is no correlation between the constituent quantities, that is, the intensity of photon emission within each of the discrete energy groups in the photon spectra. This means that all uncertainties have been added in quadrature.

The uncertainty attributed to each group-wise value in the ORIGEN-S photon spectra obtained from Tait et al. (2000), regardless of decay time and discrete energy group, was representatively chosen as 20% (Hermann and Westfall 2000; Tait et al. 1995). It is important to note that the contribution of statistical uncertainty arising from the MCNP simulation technique itself, is essentially negligible in comparison with the contribution due to uncertainty in gamma source data.

Any further modelling uncertainties introduced into the final results due to lack of an explicit representation of Zircaloy pin plugs, bearing pads, spacers and bundle end plates are judged to be minimal. The reason for this is as follows. The total mass of Zircaloy in a Bruce 37-element bundle is approximately 2.2 kg. Cladding associated with fuel elements accounts for over 85% of this mass and, as was already demonstrated, its absence increases the dose rates of interest in water by about 3%. Further, the majority of the remaining (neglected) Zircaloy mass is contained within pin plugs and end plates, which are located at the bundle ends. The bulk of the gamma radiation from fuel elements, however, is transported radially, as opposed to axially, and thus is not expected to be blocked or absorbed by the neglected Zircaloy pin plugs and end plates.

Table 5.7: Statistical uncertainty from the MCNP simulation technique and photon spectra uncertainty.

Case:	Uncertainty in Calculations as Function of Decay Time (years)*									
	10 yr.	*50 yr.*	*100 yr.*	*200 yr.*	*500 yr.*	*10^3 yr.*	*10^4 yr.*	*10^5 yr.*	*10^6 yr.*	*10^7 yr.*
MCNP Statistical Uncertainty	±0.05	±0.06	±0.06	±0.06	±0.06	±0.05	±0.05	±0.03	±0.02	±0.02
MCNP Statistical Uncertainty & 20% Uncertainty in Photon Spectra	±17.2	±19.7	±19.8	±19.8	±17.9	±17.1	±15.8	±10.4	±10.1	±10.1

*A +/- sign indicates that the dose rate in the given case is higher/lower than the nominal case.

5.3 WATER FILLED IV-324-HEX USED FUEL CONTAINER

In this section, the gamma dose rates in a water filled IV-HEX-324 used fuel container are calculated. The container, consisting of 6 layers with 54 bundles per layer arranged in a hexagonal lattice, is assumed to have failed and is thus filled with water. The density of water in the container was set to 0.9878 g/cm^3, corresponding to a temperature of 55^{o}C and a pressure of 5 MPa.

Gamma energy deposition was tracked in the following regions within the container:

- Water within each of the carbon steel tubes housing the used fuel bundles;
- Water filling the central steel tube (which does not contain any fuel bundles);
- Water between the carbon steel tubes; and
- The carbon steel vessel housing the entire bundle array.

Based on the above tallies, average dose rates in water within and outside of the inner tubes were calculated as a function of radial distance from the container centre. These dose rates were then used to calculate the F-factors, that is, the ratios of the average dose rates at particular locations within the container to the average dose rate (in water within the bundle envelope) for a single bundle in an infinite pool of water. F-factors are directly used in safety assessment models for the calculation of fuel dissolution rates.

5.3.1 IV-324-HEX Container Description

The IV-324-HEX used fuel container is a cylindrical structure consisting of two concentric cylinders. The outer cylinder, made of copper, has an outer diameter of 116.8 cm, and the inner cylinder, made of carbon steel SA516, has an outer diameter of 111.6 cm (Maak and Simmons 2001). The inner cylinder, referred to as the inner vessel, has a wall thickness of 9.6 cm (Poon et al. 2001) and houses 324 used fuel bundles, equally distributed between 6 consecutive layers. The 54 bundles in each layer are arranged in a hexagonal lattice. In order to maintain the hexagonal lattice structure, the inner vessel is furnished with 2.5 mm thick carbon steel SA210 tubes, with an outer diameter of 11.0 cm (Poon et al. 2001). Each tube runs throughout the entire length of the container and thus holds 6 bundles. The SA210 tube located at the centre of the inner vessel has a wall thickness of 12 mm and does not contain fuel bundles (Poon et al. 2001). Radial and axial container cross sections, excluding the outer copper vessel, are shown in Figures 5.2 to 5.3 below.

5.3.2 Gamma Dose Rate Calculations

For the purpose of the current calculations it was assumed that a used fuel container emplaced in deep geological repository has failed and water has filled the inner vessel. The objective of this work was then to calculate the gamma dose rates at various locations within the water filled IV-324-HEX used fuel container. This was done using MCNP gamma radiation transport calculations.

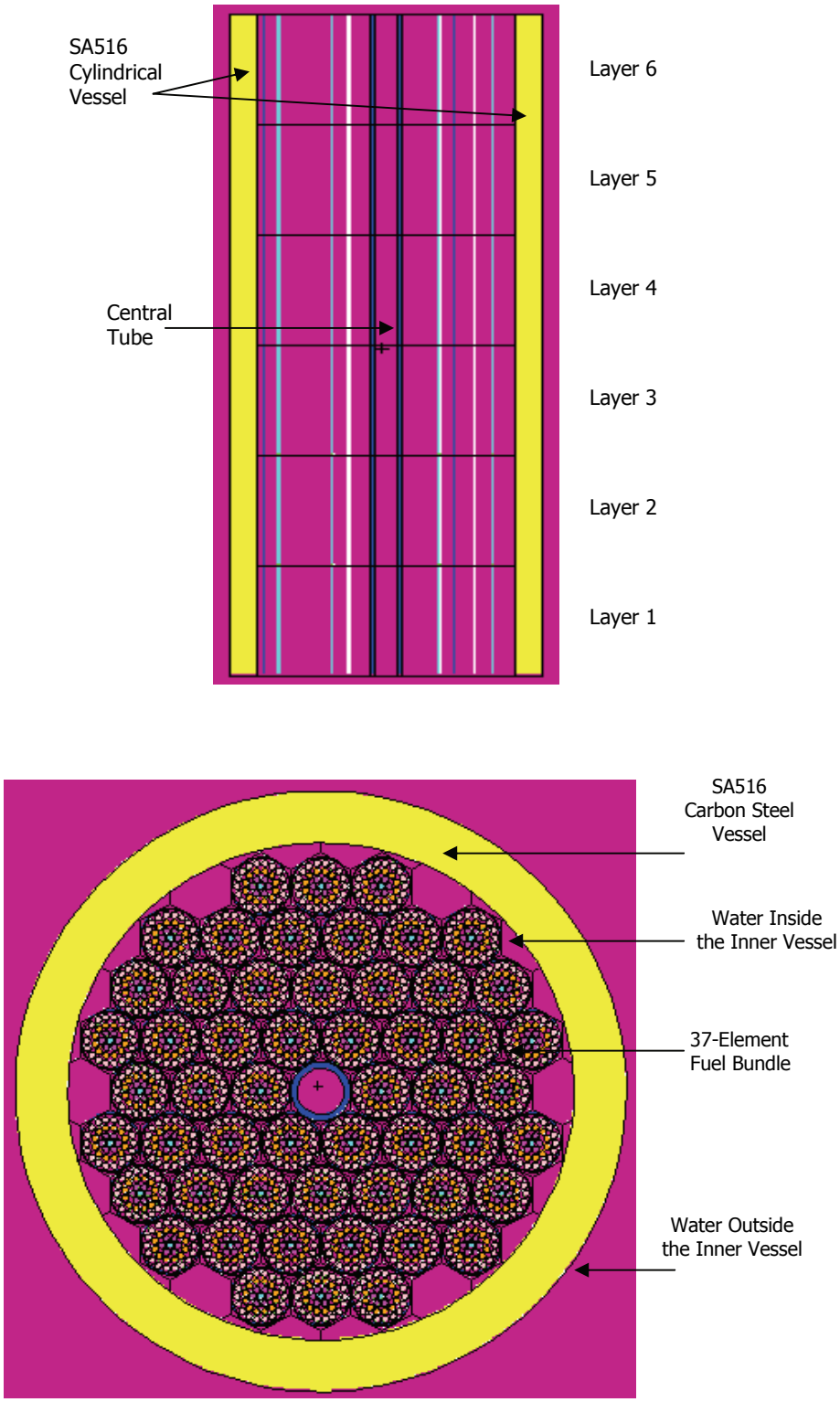

Figure 5.2: Cross section of the IV-324-HEX container: (Top) along the container length and (Bottom) in the radial direction

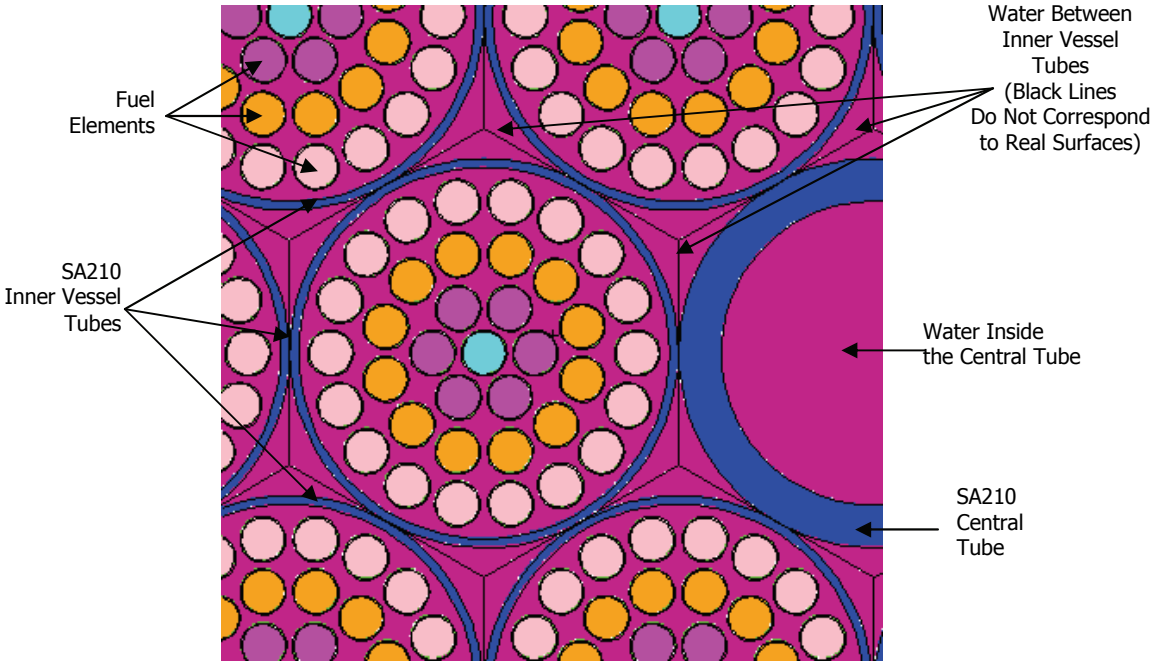

Figure 5.3: Magnified view of a fuel bundle next to the central tube in a IV-324-HEX container

As in the previous case of a single bundle (Section 5.2), a separate MCNP simulation was carried out for each of the 18 discrete energy groups shown in Table 5.1. Energy deposition was tallied separately for each layer in all fuel bundles and container components; namely, the central tube and the water contained within it, the fuel elements and cladding, the water between fuel elements, the SA210 inner vessel tubes, the water between inner vessel tubes and the cylindrical SA516 inner vessel structure and the water outside of it. The gamma energy source and the resulting energy deposition in MCNP calculation for each of the discrete energy groups was prorated to reflect the photon spectra corresponding to a fuel burnup of 220 MWh/kgU.
Dose rates in water between fuel elements were obtained as a function of radial distance from the container centre, for 7 discrete distances, and as a function of decay time.

In addition to the general assumptions stated in Section 5.1, the following assumptions apply to the current case:

- Each layer within the container is assumed to be stacked right on top of the previous layer, so that there are no water-filled spaces between the bundles in two successive layers.
- The density of water filling the used-fuel storage container is 0.9878 g/cm^3.
- The IV-324-HEX container top and bottom lids were not modelled.
- The copper vessel surrounding the steel inner vessel was not modelled.

5.3.3 Distribution of Deposited Gamma Energy Within the IV-324-HEX Container

Before discussing average dose rates in water in various parts of the used fuel container, it is instructive to have an understanding of the overall energy distribution among the various container components. The total gamma energy generated by the used fuel in the used fuel container is shown in Table 5.8.

Table 5.9 shows the distribution of deposited gamma energy inside the inner vessel, that is, the fraction of initial energy generated in used fuel deposited in fuel elements, Zircaloy cladding, water within and outside of the inner vessel tubes, as well as in the central tube and the water contained within it.

It is evident from Table 5.9 that approximately 90% of the total gamma energy generated by the used fuel bundles is dissipated in the fuel elements themselves. As in the previous calculations in Section 5.2, the decay times in the range 500 to 1000 years are characterized by a particularly 'soft' gamma photon spectrum transient (see Figure 5.1), resulting in over 99% of the total energy being deposited right within the fuel elements.

Approximately 2% to 3% of the total gamma energy, depending on the specific decay time, is deposited in Zircaloy cladding and somewhat less in the water within bundle envelopes. Bundle envelopes are, in this case, defined by the inner surface boundary of the inner vessel tubes. About 2.5% to 4% of the gamma energy is deposited in the SA210 material of the inner vessel tubes (of thickness 2.5 mm), and about 1% is deposited in water located between the tubes and within the central tube.

Comparison of the total energy fractions shown in Table 5.9 to those of the corresponding bodies in the case of a single bundle in an infinite pool of water - shown in Table 5.2 - indicates that the fraction of energy deposited in the fuel elements and the water within the bundle envelopes are higher in the used fuel container. This is expected due to the close packing of the fuel bundles, which results in absorption of energy emitted from neighbouring fuel bundles.

Table 5.9 also shows the fraction of gamma energy deposited within the 9.6 cm inner steel vessel itself and the fraction that escapes the inner steel vessel outer surfaces. The gamma energy fraction that escapes the inner steel vessel includes gamma radiation escaping from the top and bottom of the inner vessel. These data clearly show that over 97% of the total gamma photon energy is dissipated inside the inner vessel, about 1.5% to 2.5% is dissipated within the 9.6 cm thick inner steel vessel, and at most 0.1% leaves the outer surfaces of the steel vessel for decay times ranging from 10 to 10^7 years.

The gamma energy dissipated in the different water layers within the used fuel container was also examined. The gamma energy deposited in the different water layers was averaged over the symmetrically equivalent layers, that is, layers 1 and 6, layers 2 and 5, and layers 3 and 4. The results indicated that the energy deposited within each of the layers was basically identical. The total gamma energy deposited in the water within the inner vessel is shown in Table 5.8.

Table 5.8: Total gamma energy generated in the used fuel in a IV-324-HEX used fuel container and total gamma energy deposited in water within the inner vessel

	Gamma Energy (MeV/s) as a Function of Decay Time (years)									
Decay Time	10 yr.	50 yr.	100 yr.	200 yr.	500 yr.	10^3 yr.	10^4 yr.	10^5 yr.	10^6 yr.	10^7 yr.
Total Gamma Energy Generated by Used Fuel	4.22E+15	1.40E+15	4.41E+14	4.72E+13	2.89E+12	1.43E+12	1.95E+11	1.57E+11	1.77E+11	1.51E+11
Energy Deposited in Water* Within Inner Vessel	1.19E+14 (2.8%)**	3.68E+13 (2.6%)	1.15E+13 (2.6%)	1.14E+12 (2.4%)	3.80E+9 (0.1%)	2.60E+9 (0.2%)	2.77E+9 (1.4%)	4.79E+9 (3.1%)	6.51E+9 (3.7%)	6.06E+9 (4.0%)

*The mass of water in the inner vessel is approximately 1040 kg.

**Number in brackets is the percent of the total gamma energy generated in the used fuel container

Table 5.9: Distribution of the gamma energy generated in used fuel that is deposited among the various bodies within the inner vessel of the IV-324-HEX used fuel container, within the inner steel vessel itself, and escaping outside the inner vessel, assuming a fuel burnup of 220 MWh/kgU.

Body:	**Fraction of Total Energy Deposited () as a Function of Decay Time**									
	10 yr.	*50 yr.*	*100 yr.*	*200 yr.*	*500 yr.*	*10^3 yr.*	*10^4 yr.*	*10^5 yr.*	*10^6 yr.*	*10^7 yr.*
Fuel Elements	90.3 %	90.9 %	91.0 %	91.7 %	99.5 %	99.3 %	95.0 %	89.5 %	87.5 %	86.4 %
Fuel Cladding	2.3 %	2.2 %	2.2 %	2.0 %	0.2 %	0.2 %	1.3 %	2.3 %	2.6 %	2.8 %
Water Within Inner Tubes	2.0 %	1.8 %	1.8 %	1.7 %	0.1 %	0.1 %	1.0 %	2.1 %	2.5 %	2.8 %
Inner Tubes (SA210)	2.8 %	2.6 %	2.6 %	2.4 %	0.1 %	0.2 %	1.4 %	3.0 %	3.5 %	3.9 %
Water Between Inner Tubes	0.83 %	0.77 %	0.77 %	0.71 %	0.038 %	0.053 %	0.42 %	0.91 %	1.1 %	1.2 %
Central Tube (Includes Both Water &Tube)	0.18 %	0.17 %	0.17 %	0.15 %	0.0083 %	0.012 %	0.091 %	0.20 %	0.24 %	0.27 %
Inside the Inner Vessel	98.4 %	98.6 %	98.6 %	98.7 %	99.9 %	99.9 %	99.2 %	98.1 %	97.6 %	97.3 %
Within the SA516 Inner Vessel Itself	1.6 %	1.4 %	1.4 %	1.3 %	0.1 %	0.1 %	0.8 %	1.9 %	2.3 %	2.6 %
Escaping Outside the Inner Vessel Outer Walls	0.024 %	0.018 %	0.018 %	0.016 %	9.3E-4 %	0.0013 %	0.014 %	0.063 %	0.093 %	0.10 %

5.3.4 Dose Rates in Water Within the IV-324-HEX Container

This section presents average dose rates in water within bundle envelopes, that is, within the inner vessel tubes, and water immediately outside of the inner vessel tubes, as a function of radial distance, r, from the central cylindrical axis, and as a function of decay time. The 54 bundles comprising each layer were divided into 7 groups according to their distance from the central axis. These radial distances are as follows: 11.00 cm, 19.05 cm, 22.00 cm, 29.10 cm, 33.00 cm, 38.11 cm and 39.66 cm.

Dose rates in water within and immediately outside the inner vessel tubes were obtained by averaging the total deposited gamma energy over the pertinent masses of water, that is, 1.82 kg and 0.48 kg, respectively. These dose rates were calculated for every single bundle in layers 3 and 4 (i.e., the two middle layers). Following that, dose rates for bundles located at common distance from the container centreline (in both layers) were further averaged to obtain the final average dose rates.

Table 5.10 shows the average dose rates in water within the inner vessel tubes as a function of radial distance from the central axis. The highest dose rate occurs, as could be expected, in water within tubes located closest to R/2, that is, half way between the central tube and the inner surface of inner vessel. Further examination indicates that there are only minimal differences between dose rates in water in tubes at r = 19.05 cm (0.41R), r = 22.0 cm (0.48R), and r = 29.10 cm (0.63R). The differences in the dose rates for water in tubes closest to the central tube and the maxima at 0.48 R are in the range of 3 to 4%, whereas the differences between tubes closest to the inner vessel surface at 0.86R and at 0.48R range from 10 to 15%, depending on the specific decay time.

Table 5.10: Average dose rates in water within bundle envelopes as a function of radial distance, r, from the container centre. Radial distances are specified in terms of centimetres and fraction of the inner vessel inner radius, R=46.2 cm. The results are for a fuel burnup of 220 MWh/kgU.

Radial Distance From Container Centre (cm)	Dose Rates (Gy/hr) as Function of Decay Time (years)									
	10 yr.	50 yr.	100 yr.	200 yr.	500 yr.	10^3 yr.	10^4 yr.	10^5 yr.	10^6 yr.	10^7 yr.
r=11.00 (0.24 R)	8.19E+01	2.54E+01	7.91E+00	7.83E-01	2.62E-03	1.79E-03	1.90E-03	3.29E-03	4.47E-03	4.16E-03
r = 19.05 (0.41 R)	8.45E+01	2.61E+01	8.16E+00	8.07E-01	2.70E-03	1.85E-03	1.97E-03	3.41E-03	4.64E-03	4.32E-03
r = 22.00 (0.48 R)	8.46E+01	2.62E+01	8.16E+00	8.08E-01	2.70E-03	1.85E-03	1.97E-03	3.42E-03	4.65E-03	4.33E-03
r = 29.10 (0.63 R)	8.44E+01	2.61E+01	8.14E+00	8.06E-01	2.70E-03	1.84E-03	1.96E-03	3.40E-03	4.62E-03	4.30E-03
r = 33.00 (0.71 R)	8.13E+01	2.52E+01	7.85E+00	7.77E-01	2.60E-03	1.78E-03	1.89E-03	3.24E-03	4.39E-03	4.09E-03
r = 38.11 (0.82 R)	7.79E+01	2.42E+01	7.55E+00	7.47E-01	2.50E-03	1.71E-03	1.81E-03	3.07E-03	4.14E-03	3.85E-03
r = 39.66 (0.86 R)	7.53E+01	2.34E+01	7.30E+00	7.23E-01	2.42E-03	1.65E-03	1.75E-03	2.94E-03	3.96E-03	3.68E-03

Although the primary purpose of this study is to investigate gamma energy deposition in water directly adjacent to fuel elements, it is instructive to examine energy deposition in water elsewhere within the inner vessel, in order to better understand the overall pattern of energy deposition throughout the whole geometry.

Therefore, dose rates in water in close proximity to the *outer* surface of the inner tubes were also calculated. These dose rates, averaged over layers 3 and 4, are shown in Table 5.11. Since the "clusters" of water associated with each tube are concentric with the tubes themselves (see Figures 5.1 and 5.2), the corresponding dose rates are presented at the same 7 discrete radial distances as the dose rates in water between fuel elements.

Table 5.11 also shows dose rates in water within the central tube, that is, at r = 0.0 cm, and dose rates in water near the inner surface of the inner vessel, at an average radial distance r = 40.66 cm. Comparison of Tables 5.10 and 5.11 shows that the gamma dose rates in water within the inner tubes (i.e., between fuel elements) and those in water outside of the inner tubes vary from about 17% to 10% moving radially outwards from the tubes closest to the centre to about half way to the inner surface of the cylindrical vessel. From this point onward, the differences start to increase, becoming approximately 30% near the inner radius of the inner vessel.

Table 5.11: Average dose rates in water *outside* of inner tubes as a function of radial distance, r, from the container centre, in water within the central tube, and in water near inner radius periphery, r=40.66 cm. Radial distances are specified in terms of centimetres and fraction of the vessel inner radius, R=46.2 cm. Results are for a fuel burnup of 220 MWh/kgU.

Radial Distance From Container Centre (cm)	Dose Rates (Gy/hr) as Function of Decay Time (years)									
	10 yr.	*50 yr.*	*100 yr.*	*200 yr.*	*500 yr.*	*10^3 yr.*	*10^4 yr.*	*10^5 yr.*	*10^6 yr.*	*10^7 yr.*
r = 0 (Central Tube)	4.01E+01	1.21E+01	3.78E+00	3.75E-01	1.24E-03	8.46E-04	9.33E-04	1.79E-03	2.52E-03	2.36E-03
r=11.00 (0.24 R)	6.84E+01	2.10E+01	6.57E+00	6.50E-01	2.16E-03	1.48E-03	1.59E-03	2.82E-03	3.87E-03	3.60E-03
r = 19.05 (0.41 R)	7.44E+01	2.29E+01	7.15E+00	7.08E-01	2.35E-03	1.61E-03	1.73E-03	3.05E-03	4.17E-03	3.89E-03
r = 22.00 (0.48 R)	7.45E+01	2.29E+01	7.15E+00	7.08E-01	2.35E-03	1.61E-03	1.73E-03	3.06E-03	4.19E-03	3.91E-03
r = 29.10 (0.63 R)	7.41E+01	2.29E+01	7.13E+00	7.06E-01	2.34E-03	1.60E-03	1.72E-03	3.03E-03	4.14E-03	3.86E-03
r = 33.00 (0.71 R)	6.74E+01	2.08E+01	6.49E+00	6.42E-01	2.13E-03	1.46E-03	1.56E-03	2.74E-03	3.74E-03	3.49E-03
r = 38.11 (0.82 R)	5.98E+01	1.85E+01	5.76E+00	5.70E-01	1.89E-03	1.29E-03	1.39E-03	2.42E-03	3.30E-03	3.07E-03
r = 39.66 (0.86 R)	5.36E+01	1.66E+01	5.16E+00	5.11E-01	1.70E-03	1.16E-03	1.24E-03	2.17E-03	2.95E-03	2.75E-03
r = 40.66 (water near the inner radius periphery)	3.53E+01	1.09E+01	3.39E+00	3.36E-01	1.11E-03	7.63E-04	8.19E-04	1.44E-03	1.96E-03	1.83E-03

Two sets of uncertainty calculations were carried out for the dose rates shown in Table 5.10. In the first set it was assumed that the only source of uncertainty was the statistical uncertainty in the MCNP simulations. This uncertainty (one standard deviation), as is shown in Table 5.12 is ±0.1% regardless of the specific decay time or radial distance. In the second set, a 20% uncertainty was attributed to each groupwise value in the gamma photon spectra, and those uncertainties were combined along with the statistical uncertainties from the MCNP simulations. The resulting uncertainties, subject to variation with decay time, are shown in Table 5.12. The purpose of this latter set of uncertainty calculations was to contrast the difference between the uncertainties stemming from the simulation technique itself and the potential uncertainties associated with the gamma photon spectra, rather than provide a definite bound on the dose rates reported in Table 5.10.

Table 5.12: Uncertainties associated with gamma dose rates in water within inner vessel tubes, as a function of decay time.

	Uncertainty in Gamma Dose Rate in Water within the Bundle Envelope as Function of Decay Time (years)									
	10 yr.	50 yr.	100 yr.	200 yr.	500 yr.	10^3 yr.	10^4 yr.	10^5 yr.	10^6 yr.	10^7 yr.
MCNP Statistical Uncertainty	±0.1 %	±0.1 %	±0.1 %	±0.1 %	±0.1 %	±0.1 %	±0.1 %	±0.1 %	±0.1 %	±0.1 %
MCNP Uncertainty & 20 % Uncertainty in Photon Spectra	±17.0 %	±19.7 %	±19.8 %	±19.8 %	±17.9 %	±17.1 %	±15.6 %	±10.2 %	±10.3 %	±10.3 %

5.3.5 F-Factors

The F-factors are defined as the ratios of gamma dose rates in water inside the inner vessel tubes in the used fuel container (as a function of radial distance from container center), to the gamma dose rates in water within the bundle envelope for a single fuel bundle in an infinite pool of water. The results are shown Table 5.13. Since the gamma energy deposited in water within each layer of the container is the same (as previously noted), the F-factors shown in Table 5.13 are alike for all the bundle layers.

It is evident that in the radial direction the F-factors follow the pattern outlined by the dose rates in water within the bundle envelopes presented in Table 5.11. The bundle envelope water in tubes closest to R/2 is characterized by the highest F-factor. Towards the central axis, the F-factors decrease by approximately 3% to 4% with respect to those at R/2 whereas towards the inner vessel surface, the F-factors decrease by about 10% with respect to those at R/2.

The data in Table 5.13 demonstrate that between decay times of 10 and 1000 years the F-factors are approximately constant. From 1000 to 10^6 years, however, the F-factors systematically increase, before once again levelling off at 10^6 and 10^7 years.

This behaviour is a reflection of the shape of the used fuel gamma photon spectra previously discussed in Section 5.2.1. The photon spectra at decay times over 1000 years are characterized by an increased intensity of ‘high energy’ gamma photons, that is, photons with

energies above approximately 1 MeV. In the case of a single bundle in an infinite pool of water this increase does not have much impact on the energy deposited in water within the bundle envelope. This is because most of the high energy photons that penetrate the Zircaloy cladding pass through the water envelope relatively unaffected. In the case of the IV-324-HEX container, however, photons emitted outside of the fuel water envelopes can be further scattered by the SA210 inner tubes and part of that energy is eventually deposited in water within neighbouring (or the same) fuel envelopes. Thus, the F-factors at longer decay times are higher than those at the shorter decay times which are characterized by 'softer' gamma spectra.

Based on the data in Table 5.13, the weighted average (weighted by the number of fuel bundles at each radial distance) F-factor for the whole container was calculated. The weighted average F-factor for the whole container varied from 1.22 to 1.38, depending on the decay time. These values are also presented in Table 5.13.

The sensitivity of the F-factors to fuel burnup was also assessed. It was found that for fuel burnups of 280 MWh/kgU and 320 MWh/kgU the F-factors are essentially identical to those shown in Table 5.13.

The current MCNP study indicates that weighted average F-factors for the bundles within the IV-324-HEX used fuel container range from about 1.22 to about 1.38, depending on the specific decay time. For conservatism, an F-factor value of 1.4 is recommended for safety assessment calculations. This value is significantly lower than the previous estimates of the F-factor, which fell in the range of 3 to 4 (Garisto et al. 2004).

Table 5.13: F-factors for dose rates in water within the inner vessel tubes—fuel burnup 220 MWh/kgU.

Radial Distance From Container Centre (cm)	Dose Rates (Gy/hr) as Function of Decay Time (years)									
	10 yr.	50 yr.	100 yr.	200 yr.	500 yr.	10^3 yr.	10^4 yr.	10^5 yr.	10^6 yr.	10^7 yr.
r=11.00 (0.24 R)	1.26	1.24	1.24	1.24	1.24	1.24	1.26	1.35	1.40	1.40
r = 19.05 (0.41 R)	1.30	1.28	1.28	1.28	1.27	1.28	1.30	1.40	1.45	1.46
r = 22.00 (0.48 R)	1.30	1.28	1.28	1.28	1.28	1.28	1.30	1.41	1.45	1.46
r = 29.10 (0.63 R)	1.29	1.28	1.28	1.28	1.27	1.27	1.30	1.40	1.44	1.45
r = 33.00 (0.71 R)	1.25	1.23	1.23	1.23	1.23	1.23	1.25	1.33	1.37	1.38
r = 38.11 (0.82 R)	1.19	1.18	1.18	1.18	1.18	1.18	1.20	1.26	1.29	1.30
r = 39.66 (0.86 R)	1.15	1.14	1.14	1.14	1.14	1.14	1.16	1.21	1.24	1.24
Weighted Average	1.24	1.23	1.23	1.23	1.22	1.23	1.25	1.33	1.37	1.38

6. DISCUSSIONS AND CONCLUSIONS

6.1 ALPHA AND BETA DOSE RATES

The alpha and beta dose rates in water in contact with used CANDU fuel with a burnup of 220 MWh/kgU are shown in Table 6.1 as a function of decay time after discharge. Alpha and beta dose rates for higher fuel burnups are shown in Tables 3.2 and 4.1, respectively.

It should be emphasized that the alpha and beta dose rates in water decrease with distance from the fuel surface. The alpha (and beta) dose rates in water become zero at distances greater than the range of the alpha (and beta) particles in water. The average energy of the alpha and beta particles leaving the used fuel is approximately 2.5 MeV and 0.15 MeV, respectively. For these energies, the range of alpha and beta particles in water is about 13 μm and 280 μm, respectively.

Table 6.1: Average alpha and beta dose rates in water (Gy/a) in contact with used CANDU fuel with a burnup 220 MWh/kgU

Decay Time (years)	Alpha	Beta
10	1.42E+06	3.77E+06
20	1.72E+06	2.82E+06
30	1.89E+06	2.20E+06
40	1.99E+06	1.72E+06
50	2.03E+06	1.35E+06
60	2.05E+06	1.06E+06
75	2.04E+06	7.38E+05
100	2.00E+06	4.04E+05
150	1.88E+06	1.24E+05
200	1.77E+06	3.96E+04
300	1.58E+06	6.66E+03
500	1.30E+06	2.69E+03
1000	9.03E+05	1.53E+03
10^4	3.21E+05	3.78E+02
10^5	1.80E+04	1.68E+02
10^5	6.24E+03	1.49E+02
10^7	4.19E+03	1.15E+02

In addition to the calculated alpha and beta dose rates, the following observations can be made:

a) An appropriate value for the relative stopping power of alpha particles in water relative to uranium dioxide is 3.25 (with a range of 2.87 to 3.74 for alpha energies of interest).

b) The beta energy emitted by the fuel is mostly from fission products only for decay times less than about 200 years. Beyond that time, the contribution from beta decay of

actinides become increasingly significant and by 300 years is the dominant contributor to beta energy.

c) An appropriate value for the relative stopping power of beta particles in water relative to uranium dioxide is 1.8 (with a range of 1.42 to 2.09 for beta energies of interest).

The alpha and beta dose rates were calculated assuming that radionuclides are uniformly distributed in the fuel. However, it is well known that neutron flux depression occurs between rings in a fuel bundle and within a fuel element. Thus, the outer surface of the outer ring of fuel elements can be expected to have a higher burnup than the inner region of the same fuel element. The radial power profile across the rings of elements typically corresponds to differences in element linear power ratings of the order of ±20%, relative to the average for the bundle as a whole. The "skin effect" within an individual fuel element may give rise to a more pronounced variation than this, depending on the irradiation conditions.

These inter-element and intra-element effects potentially introduce variation in the nuclide concentrations near the outer surface of the fuel. These concentration variations likely represent the largest source of uncertainty in the calculation of the alpha and beta dose rates at the outer surface of a used fuel bundle.

However, the intention is to use the alpha and beta dose rates derived in this report to calculate used fuel dissolution rates for use in safety assessment studies. Generally, fuel dissolution rates are calculated making the following assumptions:

1. All used fuel in the defective used fuel container contacts water and is, therefore, dissolving (i.e., including the inner and outer elements of each fuel bundle).

   This neglects the possible protection provided by the Zircaloy cladding (Garisto et al. 2004). If the Zircaloy cladding is intact, then water would not contact the fuel and the fuel would not dissolve until after the Zircaloy cladding is breached.

2. The fuel surface area used in the calculation of the fuel dissolution rate accounts for the many cracks formed in the fuel pellets during irradiation. These cracks extend throughout the used fuel. This means that fuel dissolution occurs both at outer surfaces of the fuel and at internal crack surfaces.

Thus, the average alpha and beta dose rates in water in contact with all internal and external fuel surfaces are needed for calculating these fuel dissolution rates. In this report, these average dose rates were approximately calculated by assuming that radionuclides are uniformly distributed in the fuel.

Consequently, the main uncertainties in the calculated alpha and beta dose rates arise from the uncertainties in the radionuclide inventories used in the calculations and the variability (with particle energy) of the relative mass stopping power of alpha (Λ_α) and beta (Λ_β) particles.

The largest contributors to the alpha dose rates are Am-241, Pu-240, and Pu-239 for times less than about 10^5 years and the progeny of U-238 decay for longer times (Tait et al. 2000). The uncertainties in the inventories of Am-241, Pu-239 and Pu-240 are 20%, 4% and 3%, respectively (Garisto et al 2004). The uncertainties in the inventories of the U-238 progeny are small at long times (because these progeny are in secular equilibrium with U-238). Hence, the uncertainties in the alpha dose rates, due to uncertainties in nuclide inventories, are largest for

times less than about 1000 years, when Am-241 is the largest contributor to the alpha dose rate. During these times the uncertainty in the alpha dose rate is approximately 20%; at longer times, the uncertainty is less than 4%.

The variability of the relative mass stopping power with alpha particle energy also introduces uncertainty in the alpha dose rates. Based on this variability of the relative mass stopping power, the alpha dose rates could vary by a factor of from 0.88 to 1.15, independent of the decay time.

The largest contributors to the beta dose rates are in the order Y-90, Cs137 and Sr-90 (Tait and Hanna 2001), for times less than 300 years when the beta dose rates are largest. The uncertainties in the inventories of Y-90, Cs-137 and Sr-90 are 4%, 7% and 4%, respectively (Garisto et al 2004). Using these values, it is estimated that the uncertainties in the beta dose rates, due to uncertainties in nuclide inventories, are less than 4% for times less than 300 years.

The variability of the relative mass stopping power with beta particle energy also introduces uncertainty in the beta dose rates. Based on this variability of the relative mass stopping power, the beta dose rates could vary by a factor of from 0.79 to 1.16, independent of the decay time. This uncertainty is much larger than the uncertainty in the beta dose rates due to the uncertainties in the nuclide inventories.

6.2 GAMMA DOSE RATES

The gamma dose rates in water in contact with used CANDU fuel in a flooded IV-324-HEX used fuel container are shown in Table 6.2 as a function of decay time after discharge. These were calculated from the weighted average of the gamma dose rates in Table 5.10. Gamma dose rates for higher fuel burnups can be calculated from the gamma dose rates in Table 6.2 using data in Table 5.5.

In general, within the decay time range considered, approximately 90% of the gamma energy generated by the fuel in the IV-324-HEX container was dissipated within the UO_2 fuel matrix itself, approximately equal fractions, that is, 2-3%, were deposited within the Zircaloy cladding and water within fuel envelopes, and about 2.5% to 4% was deposited within the inner vessel tubes. However, there were exceptions at decay times between 500 and 1000 years, times characterized by relatively soft gamma photon spectra, where over 99% of the total gamma energy was deposited right within the fuel elements (see Table 5.9).

Table 6.2: Average gamma dose rates in water, within bundle envelopes, for the IV-324-HEX used container as a whole. The results are for a fuel burnup of 220 MWh/kgU

Gamma Dose Rates (Gy/a) as Function of Decay Time									
10 yr.	50 yr.	100 yr.	200 yr.	500 yr.	10^3 yr.	10^4 yr.	10^5 yr.	10^6 yr.	10^7 yr.
7.11E5	2.20E5	6.87E4	6.80E3	22.8	15.5	16.5	28.4	38.4	35.8

F-factors were also calculated. The F-factor is defined as the ratio of dose rate in water within a bundle envelope, for bundles at various locations in the IV-HEX-324 container, to the corresponding dose rate from a single bundle in an infinite pool of water. The highest values of F-factors occurred for water in tubes closest to R/2 (where R is the inner radius of the container inner vessel) and the lowest for bundles near the outer periphery of the inner vessel.

The overall range for the F-factors was determined to be 1.14 to 1.46, depending on the location of the fuel bundle in the used fuel container and the decay time. The weighted average F-factor for the used fuel container as a whole ranged from 1.22 to 1.38, depending on the decay time (see Table 5.13). An F-factor of 1.4 is recommended for safety assessment calculations.

The main uncertainty in the calculated gamma dose rates arises from the uncertainties in the gamma photon spectra, which are related to the uncertainties in the radionuclide inventories. The largest contributors to the gamma dose rates are in the order Ba-137m and Am-241 for decay times greater than 50 years (Tait and Hanna 2001). Eu-154 and Co-60 are important contributors at shorter decay times. The uncertainties in the inventories of Ba-137m and Am-241 are 7% and 20%, respectively (Garisto et al 2004). Assuming a 20% uncertainty for each groupwise value in the gamma photon spectra, the uncertainties in the gamma dose rates vary from about 20% at decay times less than about 300 years, when gamma dose rates are high, to about 10% at long decay times (see Table 5.12).

REFERENCES

Berger, M.J., J.S. Coursey, and M.A. Zucker. 2000. ESTAR, PSTAR and ASTAR: Computer programs for calculating stopping-power and range tables for electrons, protons and helium ions (version 1.2.2). National Institute of Standards and Technology, Gaithersburg, USA. [Available: http://physics.nist.gov/star]

Garisto, F. 1989. The energy spectrum of α-particles emitted from used CANDU fuel. Annals of Nuclear Energy 16, 33-38.

Garisto, F., A. D'Andrea, P. Gierszewski and T. Melnyk. 2004. Third case study - Reference data and codes. Ontario Power Generation, Nuclear Waste Management Division Report 06819-REP-01200-10107-R00. Toronto, Canada.

Hermann, O.W. and R.M. Westfall. 2000. ORIGEN-S: Scale system module to calculate fuel depletion, actinide transmutation, fission product buildup and decay, and associated radiation terms. U.S. Nuclear Regulatory Commission Report NUREG/CR-0200, Revision 6, Volume 2. Washington DC, USA.

International Commission on Radiation Units and Measurements (ICRU). 1984. Stopping powers for electrons and positrons. ICRU Report 37. Vienna, Austria.

International Commission on Radiation Units and Measurements (ICRU). 1993. Stopping powers and ranges for protons and alpha particles. ICRU Report 49. Vienna, Austria.

Kocher, D.C. (J.S. Smith, editor). 1981. Radioactive decay tables. A handbook of decay data for application to radiation dosimetry and radiological assessments. Oak Ridge National Laboratory Report DOE/TIC-11026. Oak Ridge, USA.

Maak, P. and G. Simmons. 2001. Summary report: A screening study of used-fuel container geometric designs and emplacement methods for a deep geologic repository. Ontario Power Generation Report 06819-REP-01200-10065-R00. Toronto, Canada.

Nitzki, V. and Hj. Matzke. 1973. Stopping power of 1-9 MeV He^{++} ions in UO_2, $(U,Pu)O_2$, and ThO_2. Physics Review B 8, 1894-1900.

Poon, G., M. Saiedfar and P. Maak. 2001. Selection of a primary load-bearing component conceptual design for used-fuel containers. Ontario Power Generation, Nuclear Waste Management Division Report 06819-REP-01200-10051-R00. Toronto, Canada

Sunder, S. 1995. Alpha, beta and gamma dose rates in water in contact with used CANDU UO_2 fuel. Atomic Energy of Canada Limited Report AECL-11380, COG-95-340. Pinawa, Canada.

Sunder, S. 1998. Calculation of radiation dose rates in a water layer in contact with used CANDU UO_2 fuel. Nuclear Technology 122, 211-221.

Tait, J.C., I.C. Gauld and A.H. Kerr. 1995. Validation of the ORIGEN-S code for predicting radionuclide inventories in used CANDU fuel. J. Nucl. Mat. 223, 109-121.

Tait, J.C., H. Roman and C.A. Morrison. 2000. Characteristics and radionuclide inventories of used fuel from OPG nuclear generating stations. Volume 1 – Main Report and Volume 2 - Radionuclide inventory data. Ontario Power Generation, Nuclear Waste Management Division Report 06819-REP-01200-10029-R00. Toronto, Canada

Tait, J.C. and S. Hanna. 2001. Characteristics and radionuclide inventories of used fuel from OPG nuclear generating stations. Volume 3 – Radionuclide inventory data. Decay times 10 to 300 years. Ontario Power Generation, Nuclear Waste Management Division Report 06819-REP-01200-10029-R00. Toronto, Canada

X-5 Monte Carlo Team. 2003. MCNP – A general Monte Carlo N-particle transport code, version 5. Volume 1: Overview and theory. Los Alamos National Laboratory Report LA-UR-03-1987. Los Alamos, USA.

APPENDIX: MATERIAL COMPOSITIONS

Zircaloy Cladding:

Element	Wt. Frac. (%)
Zr	9.97E+01
Fe	2.13E-01
Cr	1.02E-01
Ni	7.13E-03
B	6.53E-05

Fuel composition varied with each of the four fuel rings. The composition shown in the following table corresponds to the outermost fuel ring.

Element	Wt. Frac. (%)
U	8.72E+01
O	1.19E+01
Pu	4.04E-01
Nd	8.31E-02
Mo	6.79E-02
Ce	5.34E-02
Ru	4.75E-02
Cs	3.66E-02
La	3.29E-02
Pr	2.75E-02
Pd	2.31E-02
Tc	2.26E-02

Carbon Steel SA210 – Density 7.85 g/cm^3.

Element	Wt. Frac.
Fe	0.9863
Mn	0.0093
C	0.0027
Si	0.001
P	0.00035
S	0.00035

Carbon Steel SA516 – Density 7.85 g/cm^3.

Element	Wt. Frac.
Fe	0.9811
Mn	0.012
Si	0.004
C	0.0022
P	0.00035
S	0.00035